

1 **GARRLiC and LIRIC: strengths and limitations for the**
2 **characterization of dust and marine particles along with**
3 **their mixtures**

4
5 **Alexandra Tsekeri¹, Anton Lopatin², Vassilis Amiridis¹, Eleni Marinou^{1,3}, Julia**
6 **Igloffstein⁴, Nikolaos Siomos³, Stavros Solomos¹, Panagiotis Kokkalis¹, Ronny**
7 **Engelmann⁴, Holger Baars⁴, Myrto Gratsea⁵, Panagiotis I. Raptis^{5,6}, Ioannis**
8 **Biniotoglou⁷, Nikolaos Mihalopoulos^{5,8}, Nikolaos Kalivitis^{1,8}, Giorgos**
9 **Kouvarakis⁸, Nikolaos Bartsotas⁹, George Kallos⁹, Sara Basart¹⁰, Dirk**
10 **Schuettemeyer¹¹, Ulla Wandinger⁴, Albert Ansmann⁴, Anatoli P. Chaikovsky¹²,**
11 **and Oleg Dubovik²**

12 [1]{Institute for Astronomy, Astrophysics, Space Applications and Remote Sensing, National
13 Observatory of Athens, Athens, Greece }

14 [2]{Laboratoire d' Optique Atmosphérique, Université de Lille, Lille, France }

15 [3] {Laboratory of atmospheric physics, Physics Department, Aristotle University of
16 Thessaloniki, Greece }

17 [4]{Leibniz Institute for Tropospheric Research, Leipzig, Germany }

18 [5]{IERSD, National Observatory of Athens, Athens, Greece }

19 [6]{Physikalisch-Meteorologisches Observatorium Davos/World Radiation Center
20 (PMOD/WRC), Davos Dorf, Switzerland }

21 [7]{National Institute of R&D for Optoelectronics, Magurele, Ilfov, Romania }

22 [8]{Environmental Chemical Processes Laboratory, University of Crete, Heraklion, Greece }

23 [9]{University of Athens, School of Physics, Athens, Greece }

24 [10]{Barcelona Supercomputing Center, Barcelona, Spain }

25 [11]{European Space Agency }

26 [12]{Institute of Physics, NAS of Belarus, Minsk, Belarus }

27 Correspondence to: Alexandra Tsekeri (atsekeri@noa.gr)

1 **Abstract**

2 The **Generalized Aerosol Retrieval from Radiometer and Lidar Combined** data algorithm
3 (**GARRLiC**) and the **Lidar-Radiometer Inversion Code (LIRIC)** provide the opportunity to
4 study the aerosol vertical distribution by combining ground-based lidar and sun-photometric
5 measurements. Here, we utilize the capabilities of both algorithms for the characterization of
6 Saharan dust and marine particles, along with their mixtures, in the South-Eastern
7 Mediterranean during the “**CHARacterization of Aerosol mixtures of Dust and Marine origin**
8 **Experiment (CHARADMEExp)**”. Three case studies are presented, focusing on dust-dominated,
9 marine-dominated and dust/marine mixing conditions. **GARRLiC** and **LIRIC** achieve a
10 satisfactory characterization for the dust-dominated case in terms of particle microphysical
11 properties and concentration profiles. The marine-dominated and the mixture cases are more
12 challenging for both algorithms, although **GARRLiC** manages to provide more detailed
13 microphysical retrievals compared to **AERONET**, while **LIRIC** effectively discriminates dust
14 and marine in its concentration profile retrievals. The results are also compared with modelled
15 dust and marine concentration profiles and surface in situ measurements.

16

17 **1 Introduction**

18 The importance of studying the vertical distribution of aerosol plumes is prominent in regional
19 and climate studies, since it can effectively change the radiative properties of the atmosphere
20 and the presence of clouds (e.g. Pérez et al., 2006a; Solomon et al., 2007). Ground-based
21 monitoring of the aerosol vertical structure is effectively performed with the synergy of passive
22 and active remote sensing instruments, in particular with multi-wavelength sun-photometers
23 and lidars. The sun-photometer provides the columnar properties of the particles (e.g. Dubovik
24 and King, 2000a; Dubovik et al., 2006), whereas the lidar is capable of providing vertical
25 profiles of the backscatter and extinction coefficients, along with vertical profiles of the particle
26 microphysical properties, mainly for the fine mode (e.g. Müller et al., 2016). The combination
27 of active with passive remote sensing has been tried so far mostly by using the sun-photometer
28 measured aerosol optical depth (AOD) as ancillary information for the lidar retrieval (e.g.
29 Fernald et al., 1972; Ansmann et al., 2011; 2012). **GARRLiC** (Lopatin et al., 2013) and **LIRIC**
30 (Chaikovsky et al., 2016) algorithms go a step further and use deeper synergies: the **LIRIC**
31 approach derives the particle concentration profiles from the lidar measurements, considering

1 the columnar microphysical properties derived separately from the sun-photometer; GARRLiC
2 advances the method even more, combining for the first time both sun-photometer and lidar
3 measurements for the retrieval of the particle microphysical properties. As discussed in detail
4 in Lopatin et al. (2013), combining the sun-photometer intensity measurements with the
5 backscatter lidar information seems to result in better sensitivity to the particle shape, as well
6 as the ability to retrieve the refractive indices of fine and coarse particles separately, along with
7 extracting the vertical distribution of the fine and coarse particle concentrations. Moreover, it
8 can potentially provide higher accuracy for cases of low aerosol loadings, compared with the
9 intensity-only retrieval.

10 GARRLiC and LIRIC have been developed in the framework of the Aerosols, Clouds and Trace
11 gases Research Infrastructure (ACTRIS, <http://www.actris.eu/>), utilizing the capabilities of
12 combined European stations of the AErosol RObotic NETwork (AERONET, Holben et al.,
13 1998) and the European Aerosol Research Lidar Network (EARLINET, Pappalardo et al.,
14 2014). Both algorithms have been tested for a variety of aerosol types and their mixtures. For
15 example, LIRIC has been tested for dust and volcanic aerosols (Wagner et al., 2013),
16 dust/pollution mixture (Tsekeri et al., 2013), dust, pollution and mixture of dust/smoke and
17 pollution (Granados-Muñoz et al., 2014; 2015; Papayannis et al., 2014), and smoke/pollution
18 mixture (Kokkalis et al., 2016). LIRIC has also been used to study dust transport events and
19 dust modeling performance over Europe (Biniotoglou et al. 2015, Granados-Munoz, 2016), as
20 well as to evaluate air quality models (Siomos, et al. 2017). GARRLiC has been tested for dust
21 and smoke (Lopatin et al., 2013) and dust aerosols (Bovchaliuk et al., 2016).

22 GARRLiC and LIRIC input and output data is shown in Fig. 1, while short descriptions are
23 given herein: LIRIC algorithm uses the particle microphysical properties provided in the
24 AERONET product as a-priori information in the inversion of the lidar measurements for
25 retrieving the aerosol volume concentration profiles. Using lidar measurements of elastic
26 backscatter at three wavelengths of 355, 532, and 1064 nm, LIRIC retrieves the volume
27 concentration profiles of fine and coarse particles. Moreover, the cross-polarized lidar signal at
28 532 nm allows the decoupling of the coarse mode into its spherical and non-spherical
29 components. The error estimation of the retrieved profiles is provided as well. Both LIRIC and
30 GARRLiC retrievals assume that key aerosol properties vary smoothly (e.g. aerosol
31 concentration varies smoothly with height), but otherwise do not constrain the absolute values
32 of the retrieved quantities. In this way the algorithms exclude solutions that are mathematically

1 possible, but contain unrealistic oscillations in the retrieved properties (see also Dubovik, 2004;
2 Dubovik and King, 2000). GARRLiC algorithm synergistically combines the sun-photometer
3 sun and sky measurements at four wavelengths (at 440, 670, 870 and 1020 nm) and up to 35
4 scattering angles, with the vertically-resolved lidar measurements of the elastic backscatter at
5 three wavelengths (at 355, 532, and 1064 nm). The algorithm does not use the AERONET
6 products, but it instead calculates the size distribution, spherical particle fraction and spectral
7 complex refractive index, separately for fine and coarse particles. In case of a dominant mode
8 (e.g. for pure dust cases), the algorithm is set to retrieve the aerosol characteristics for one mode
9 only. Although in GARRLiC the microphysical properties are considered to be constant along
10 the column for each mode, the total values change along the column in case of two modes with
11 different properties. The algorithm calculates also the volume concentration profiles of fine and
12 coarse particles. The concentrations are considered constant below the lowest height of the lidar
13 signals, which may introduce errors in the retrieved profiles (e.g. Tsekeri et al., 2013). The
14 retrieval uncertainties of the microphysical parameters are provided as well, following the
15 approach described by Dubovik et al. (2000) and the profile retrieval uncertainties are currently
16 under development. GARRLiC and its updates are available for download at [http://www.grasp-
17 open.com/doc/ch04.php#grasp-manager](http://www.grasp-open.com/doc/ch04.php#grasp-manager), as part of the GRASP code (Dubovik et al., 2014).

18 In case of multi-mode aerosol mixtures and/or change of microphysical properties with height
19 due to particle hygroscopic growth (e.g. Tsekeri et al., 2017) an inherent deficiency of both
20 algorithms is the number of aerosol modes retrieved, with LIRIC considering three modes (fine
21 particles, coarse spherical and coarse non-spherical particles) and GARRLiC considering two
22 modes (fine and coarse particles). We need to highlight here that LIRIC retrieves three modes
23 only for the volume concentration profiles, whereas otherwise it uses the AERONET products,
24 providing for example a common spectral refractive index for all modes (Fig. 1). Both
25 algorithms work well for individual aerosol components or mixtures of (mainly) fine (e.g.
26 pollution) and (mainly) coarse (e.g. dust) particles, but they should not be able to fully
27 characterize the mixture components in case of more than one fine or coarse mode in the
28 mixture, as in smoke/pollution or dust/marine mixture cases. For the latter, LIRIC should
29 provide an effective characterization for the volume concentration profiles, since it derives the
30 coarse spherical (hydrated marine) particles and the non-spherical (dust) particles, but the
31 characterization is not expected to be satisfactory for the particle microphysical properties.

1 In our study, we apply GARRLiC and LIRIC for cases of dust, marine and a dust/marine
2 mixture during the CHARADME_{Exp} campaign in the South-Eastern Mediterranean. This is the
3 first time a detailed characterization of marine and marine mixtures with dust along the
4 atmospheric column is performed for the area. So far, various studies have tried to characterize
5 the aerosol radiative properties in the Mediterranean with satellite or ground-based AOD
6 measurements (e.g. di Sarra et al., 2008; Kazadzis et al., 2009; Papadimas et al., 2012).
7 Unfortunately, they fail to overcome their limitations such as the non-realistic assumptions for
8 the aerosol absorption properties and the lack of information of the real vertical aerosol structure
9 (Mishra et al., 2014). The kind of characterization presented here is important for application
10 in future satellite missions not only for the Mediterranean, but for large parts of the globe where
11 dust and marine particles are present, as in the Atlantic Ocean (e.g. Prospero, 1996).

12 The CHARADME_{Exp} campaign and the three cases (i.e. mainly dust, marine/pollution mixture
13 and dust/marine/pollution mixture) are presented in section 2. The methodology followed in
14 our work is presented in section 3, the GARRLiC and LIRIC results are shown in section 4 and
15 finally our conclusions are given in section 5.

16

17 **2 Overview of the CHARADME_{Exp} campaign and datasets**

18 CHARADME_{Exp} was an experimental campaign of ESA, implemented by the National
19 Observatory of Athens (NOA), aiming at the characterization of dust and marine particles along
20 with their mixtures (<http://charadmexp.gr>). The campaign took place at the ACTRIS Finokalia
21 station (35.338°N, 25.670°E) on the north coast of Crete, in Greece (Fig. 2), from 20 June to
22 20 July 2014. The station is situated at the top of a hilly elevation (252 m above sea level) and
23 it is a background site with no human activities occurring at a distance shorter than 15 km,
24 making the station ideal for monitoring natural aerosols mainly of desert and marine origin. The
25 area is characterized by the existence of two well-distinguished seasons equally distributed
26 throughout the year: the dry season from April to September and the wet season from October
27 to April, with the first one characterized mainly by winds of N/NW direction (Central and
28 Eastern Europe and Balkans) carrying smoke and long range transported anthropogenic
29 pollution to the area (Sciare et al., 2008; Vrekoussis et al., 2005), and the second one with less
30 pronounced N/NW winds and important transport from the Sahara desert (S/SW winds;
31 occurrence up to 20%). Dust transport, while less frequent during the dry period, it is still

1 observed (e.g. Papadimas et al., 2005) and is characterized by a transportation pattern through
2 the free troposphere and weaker vertical mixing of the dust layers (e.g. Kalivitis et al., 2007).

3 **2.1 Instruments and methods**

4 **2.1.1 Lidar**

5 The Polly^{XT} OCEANET lidar (Engelmann et al., 2016) operated at a 24/7 basis during
6 CHARADME_{Exp}, measuring aerosol loads in the boundary layer and the free troposphere. The
7 system was provided by the Leibniz Institute for Tropospheric Research (TROPOS -
8 <http://www.tropos.de>). It employs 3 backscatter channels (at 355, 532 and 1064 nm), 2 Raman
9 extinction channels (at 387 and at 607 nm), 2 depolarization channels (at 355 and 532 nm) and
10 one water–vapor channel (at 407 nm). The lidar is housed in a container and can be operated
11 under various climatic conditions. The full description of the original lidar system can be found
12 in Althausen et al. (2009) and in Engelmann et al. (2016). More about the network of Polly
13 systems (i.e., Polly^{NET}) can be found in Baars et al. (2016).

14 The information close to the surface is very important for our study, especially for the marine
15 particle characterization, since the marine particles reside mostly below 1 km (e.g. Ho et al.,
16 2015). Unfortunately, this is also the lidar “overlap region”, with large uncertainty for the lidar
17 backscattered signal due to its partial collection from the telescope (e.g. Wandinger and
18 Ansmann, 2002). Polly^{XT} OCEANET far-field (FF) signal full overlap is at ~800 m (Engelmann
19 et al., 2016) and it operates two near–field (NF) channels utilizing a separate 50–mm refractor
20 telescope at a distance of 120 mm from the axis of the laser beam, providing a full overlap at
21 150 m above surface at 532 and 607 nm. The NF measurements are not used in GARRLiC and
22 LIRIC, since both algorithms require the complete set of wavelengths provided by the lidar
23 during CHARADME_{Exp} only for the FF measurements. Nevertheless, we use the NF
24 measurements to perform overlap correction in the FF signals, as described in Engelmann et al.
25 (2016) and this allowed us to use the FF-corrected lidar signals from ~550 m, instead of 800 m.
26 In future efforts we plan to utilize the additional information provided by our new Polly^{XT} lidar
27 system currently installed at Finokalia station, measuring NF signals at both 355 and 532 nm,
28 by performing the signal gluing technique for NF and FF signals at 355 and 532 nm and overlap
29 correction for the FF signal at 1064 nm.

1 **2.1.2 Sun-photometer**

2 The CIMEL CE318 sun-photometer is the instrument used in the AERONET sun-photometer
3 network, with more than 250 units worldwide. The technical specifications of the instrument
4 are given in detail by Holben et al. (1998). Taking into account all the information about the
5 instrument and calibration precision (Holben et al., 1998) the accuracy of the AOD
6 measurements is estimated to be of the order of ± 0.02 in the UV and ± 0.01 in the visible range
7 regarding the level 2 (cloud-screened and quality-assured) data. In the current analysis we
8 utilized the level 1.5 products (i.e., automatically cloud cleared but may not have final
9 calibration applied) for the LIRIC retrieval, since the level 2 data were not available in the time
10 ranges selected for the retrievals. For the GARRLiC retrieval we used the sun and sky multi-
11 angle measurements at four wavelengths (440, 670, 870 and 1020 nm) (Dubovik and King,
12 2000).

13 **2.1.3 Surface in situ**

14 The GARRLiC retrieved size distribution is evaluated against the surface measurements of the
15 Scanning Mobility Particle Spectrometer (SMPS). SMPS provides the fine particle number size
16 distribution at $\sim 9 - 848$ nm (nominal) radius. Unfortunately, there were no size distribution
17 measurements for the coarse particles at Finokalia station during CHARADMEp. Note that
18 for a direct comparison of SMPS number size distribution (in cm^{-3}) with the GARRLiC
19 volume size distribution retrievals (in $\mu\text{m}^3 \mu\text{m}^{-2}$) we first have to calculate the SMPS volume
20 size distribution (in $\mu\text{m}^3 \text{cm}^{-3}$) and then to multiply it with the height extent of fine particles in
21 the column, derived by the collocated lidar measurements.

22 Moreover, we evaluate the particle concentration derived from GARRLiC and LIRIC at the
23 surface level with the surface in situ measurements of the particular matter for particles with
24 diameters less than $10 \mu\text{m}$ (PM_{10}). The PM_{10} is continuously measured at Finokalia station with
25 an Eberline FH 62 I-R (Eberline Instruments GmbH) particulate monitor (Gerasopoulos et al.,
26 2006). GARRLiC and LIRIC retrieve the particle concentration for a wider size range (up to 15
27 μm in radius, or $30 \mu\text{m}$ in diameter), thus their PM_{10} values are calculated using the respective
28 volume percentages for particles with radius less than $5 \mu\text{m}$.

29 In order to compare the in situ measured size distribution and mass concentration with
30 GARRLiC and LIRIC ambient retrievals, we need to take into account the particle drying
31 applied to surface measurements. The in situ instruments dry the sampled air by adiabatic

1 compression during the sampling through their inlets and by the radiant heat from the lights
2 inside the instruments. The size and mass of the ambient particles thus changes, especially in
3 case of hygroscopic particles in humid conditions (e.g. Snider and Petters, 2008). For the size
4 distribution we evaluate this effect qualitatively (see section 4.2 and 4.3). For the PM_{10}
5 comparison we calculate the “dry” GARRLiC and LIRIC PM_{10} , using the particle hygroscopic
6 growth (i.e., the ratio of the ambient to dry particle size, f_g) as shown in Eq. 1:

$$PM_{10d} = f_g^{-3} PM_{10a} \quad (1)$$

7 where d and a denote the dry and ambient particles, respectively.

8 We derive f_g for different relative humidity (RH) values using the hygroscopicity parameter κ
9 (Petters and Kreidenweis, 2007) as shown in Eq. 2:

$$f_g = \left(1 + \kappa \frac{RH}{100 - RH} \right)^{\frac{1}{3}} \quad (2)$$

10 For the cases analysed herein, we consider a κ value of 0.4 to be characteristic for particles in
11 the south-eastern Aegean Sea (Bezantakos et al., 2013). A more detailed treatment of comparing
12 dry in situ measurements with ambient remote sensing retrievals is out of the scope of this
13 analysis, but it is very important when combining these different techniques (e.g. Tsekeri et al.,
14 2017).

15 **2.2 Models**

16 **2.2.1 Source-receptor analysis**

17 The origin of the examined aerosol layers at the Finokalia station is investigated with the use
18 of source-receptor computations derived with dispersion modelling tools. The corresponding
19 emission sensitivity (i.e. the residence time of the tracer particles inside the lowest tropospheric
20 layers) is calculated from backward Lagrangian simulations with the atmospheric dispersion
21 model FLEXPART-WRF (Brioude et al., 2013). The dispersion model is offline coupled with
22 the WRF_ARW atmospheric model (Skamarock et al., 2008). The spatial resolution of WRF is
23 12×12 km and we use its hourly outputs to drive the FLEXPART runs. This configuration
24 allows the simulation of meso- γ scale circulations that play an important role for the planetary
25 boundary layer properties and for the regional and local scale transport of the particles. The
26 backward FLEXPART runs are performed for 5-day periods and we assume a release of 40000

1 tracer particles from each arriving layer over the Finokalia station. The modelled retroplume
2 maps show the spatial distribution of the tracer particle residence time below 1 km. Thus, the
3 areas showing longer residence times in these maps indicate the source areas/origin of the
4 particles arriving at the specific heights above Finokalia station.

5 **2.2.2 Desert dust model**

6 Desert dust emissions and transport are described with the BSC-DREAM8b model (Nickovic
7 et al., 2012; Pérez et al., 2006a; Basart et al., 2012a). The BSC-DREAM8b model is embedded
8 into the Eta/NCEP atmospheric model and solves the mass balance equation for dust, taking
9 into account the different processes of the dust cycle (i.e., dust emission, transport and
10 deposition). The updated version of the model includes a source function based on the 1 km
11 USGS land use data, 8 particle size bins (0.1–10 μm radius range), and dust-radiative
12 feedbacks. The present analysis utilize the BSC-DREAM8b dust simulations for the period from
13 20 June to 20 July 2014 with hourly output. The initial state of dust concentration in the model
14 is defined by the 24 h forecast from the previous day model run. The NCEP Final Analyses (at
15 $1^\circ \times 1^\circ$ horizontal resolution) at 00:00 UTC are used as initial conditions and boundary
16 conditions at intervals of 6 h. Moreover, the model configuration includes 24 Eta vertical layers
17 extending up to approximately 15 km in the vertical. The resolution is set to 0.33° in the
18 horizontal.

19 **2.2.3 Sea-salt model**

20 Sea salt emissions and transport are described with the atmospheric model RAMS-ICLAMS
21 (Solomos et al., 2011). The model is an enhanced version of RAMS (Pielke et al., 1992; Cotton
22 et al., 2003) and it includes a full description of the sea salt lifecycle in the atmosphere. The
23 parameterization of sea salt emission is based on the white-cap formation for the entrainment
24 of sea salt spray in the atmosphere (Monahan et al., 1986), taking also into account the effects
25 of RH on the size distribution of the particles (Zhang et al. 2005). Sea salt flux close to the
26 coastline is also calculated in the model following the parameterizations of Leeuw et al. (2000)
27 and Gong et al. (2002). The dry and wet removal processes are treated with the corresponding
28 schemes described in Seinfeld and Pandis (1998). The simulated sea salt mass is represented
29 with a bimodal lognormal distribution. The first (accumulated) mode has a mean diameter of
30 $0.36 \mu\text{m}$ and a geometric dispersion of 1.80. The second (coarse) mode has a mean diameter
31 of $2.85 \mu\text{m}$ and the geometric dispersion is 1.90.

1

2 **3 Results**

3 In order to demonstrate the GARRLiC and LIRIC capabilities in characterizing events with dust
4 and marine particles, we analyse in detail three cases acquired during CHARADMExp at
5 Finokalia. The first case is a relatively moderate dust episode with low amount of marine and
6 continental particles, the second is a low-AOD marine and continental plume and the last is a
7 mixture of dust, marine and continental particles. Source-receptor simulations are used to derive
8 the particle origin and characterize the air masses. Then, we compare the optical properties
9 retrieved from GARRLiC, LIRIC and collocated Klett retrievals (Klett, 1985). The GARRLiC
10 and LIRIC/AERONET fine mode size distributions and PM₁₀ concentrations are compared with
11 surface in situ measurements. Finally, the dust and marine concentration profiles are compared
12 with the corresponding profiles from BSC-DREAM8b and RAMS-ICLAMS models.

13 **3.1 Dust-dominated case**

14 On June 26 the Polly^{XT} measurements of volume depolarization ratio at 532 nm showed the
15 advection of non-spherical particles (volume depolarization ratio at 532 nm of 0.15-0.2), at
16 height ranges extending from close to the ground up to 5-6 km (Fig. 3a) and an AOD at 440 nm
17 of 0.4. Model simulations also support our observations: dust transport simulations using the
18 BSC DREAM8b model indicate Saharan dust transport to Finokalia. As shown by the
19 FLEXPART footprints in Fig. 3b, the particles reaching from the ground up to 2 km have
20 possible near-surface sources at the West Sahara region, with potential mixing of marine and
21 continental particles from the western Mediterranean region, the Balkans and Greece, while the
22 particles arriving at 3-6 km are most likely dust from the Sahara desert between 0°-10° E and
23 25°-35° N. The presence of dust particles is indicated from AERONET as well, with Ångstrom
24 exponent at 440/870 nm of ~0.1, sphericity parameter <2.3 % and a coarse-mode dominated
25 size distribution. These values are characteristic for dust particles, as reported in the 8-year
26 global AERONET climatology of Dubovik et al. (2002).

27 Considering that the atmospheric column is dominated by dust (as shown in the coarse mode
28 dominated AERONET size distribution), we performed the one-mode GARRLiC inversion.
29 For both GARRLiC and LIRIC we used the lidar measurements at 4-6 UTC (red box in Fig.
30 3a) and the sun-photometer measurements at 4:54 UTC. Our results show that GARRLiC and
31 LIRIC backscatter and extinction coefficient profiles at 355, 532 and 1064 nm agree quite well,

1 with their differences being 10-20% with respect to GARRLiC values, well within the LIRIC
2 uncertainties (Fig. 4a and b). Larger differences are seen below ~550 m, in the lidar incomplete
3 overlap region. Figure 4 shows also the comparison of GARRLiC backscatter and extinction
4 coefficients with the ones produced with the Klett method (Klett, 1985). The Klett profiles are
5 restricted to 5 km, since the low signal to noise ratio of the day-time lidar measurements
6 introduces large uncertainty to the Klett retrievals above that height. For the Klett retrievals we
7 used an extinction-to-backscatter ratio, or “lidar ratio” (LR) of 40 sr for 532 and 1064 nm and
8 of 47 sr for 355 nm, which result in extinction coefficient profiles that closely reproduce the
9 sun-photometer-measured AODs at 340, 500 and 1020 nm (i.e. 0.42, 0.42 and 0.38),
10 respectively. The uncertainty in the assumed lidar ratios are taken into account by considering
11 a 20 % uncertainty in the backscatter retrievals (Fig. 4c). The agreement of GARRLiC with
12 Klett retrievals is considered satisfactory, with differences for the backscatter coefficient to be
13 within the Klett retrieval uncertainty, and for the extinction coefficient to be less than 30% at
14 heights above 550 m (Fig. 4d). Figure 4d shows also the NF retrievals at 532 nm, providing
15 information of the particle properties down to 150 m. In particular, we see a decrease in the
16 particle backscatter and extinction coefficients near the surface, which is not retrieved by
17 GARRLiC or LIRIC due to missing NF information as discussed in section 3.1.1.

18 A special feature seen in GARRLiC, LIRIC and Klett backscatter profiles is the larger
19 backscatter at 532 than 355 nm. This is not usual for dust particles, but it has been reported
20 before: Veselovskii et al. (2016) have shown a similar spectral dependence for dust during the
21 study of SaHAran Dust Over West Africa (SHADOW) campaign, which they attributed to large
22 dust particle spectral variation of the imaginary part of the refractive index. More specifically,
23 they managed to reproduce this backscatter spectral dependence with imaginary part values of
24 ~0.01 at 355 nm and 0.005 at 532 nm. Although these values are not the same with the retrieved
25 0.001 at 355 nm and 0.0005 at 532 nm for our case (Fig. 5 –bottom, right), the backscatter
26 spectral dependence can be a combination of the effect that different factors have on the
27 backscattered light, as the size or shape of the dust particles.

28 Figure 5 shows good agreement between GARRLiC and AERONET retrievals (the latter used
29 in the LIRIC retrieval), within the GARRLiC retrieval uncertainties. Differences are seen only
30 for the real part of the refractive index, which for GARRLiC is at ~1.45, at the low end of the
31 dust climatological value range of 1.48 ± 0.05 - 1.56 ± 0.03 as reported in Dubovik et al. (2002).
32 This value though is much lower than expected for dust from West Sahara in situ measurements,

1 reporting values of 1.55-1.65 (e.g. Kandler et al., 2007), and it may be due to the marine particle
2 mixture at lower heights, with real part of refractive index of ~ 1.35 . The same is true for the
3 low values of the imaginary part, due to the mixture of dust with imaginary part of e.g. 0.05 at
4 532 nm (e.g. Wagner et al., 2012) and marine particles with imaginary part of ~ 0.0005 at 532
5 nm (e.g. Babin et al., 2003). Nevertheless, an important feature of the GARRLiC retrieval is
6 the spectral dependence of the single scattering albedo (SSA), showing the characteristic
7 increase of dust absorption in the ultraviolet (Fig. 5, up right) (Otto et al., 2007). Moreover, the
8 GARRLiC size distribution agrees well with surface in situ SMPS measurements for the fine
9 mode, showing a very small volume concentration for fine particles. The SMPS number size
10 distribution is converted to $\mu\text{m}^3\mu\text{m}^{-2}$ for a direct comparison with the GARRLiC and
11 AERONET product, as described in section 2.1.3: For this conversion we consider that mainly
12 the first 2 km contain fine particles due to the mixing of marine and continental particles with
13 dust there (Fig. 3b). Moreover, due to the low RH at the surface (16%) we do not expect
14 differences between the GARRLiC ambient size distribution and the SMPS dry measurements.

15 The concentration profiles from GARRLiC and LIRIC are in excellent agreement at heights >1
16 km, with differences to be less than 10% (Fig. 6a). LIRIC retrieves fine and coarse mode
17 profiles, whereas GARRLiC considers only one mode, dominated by coarse particles. The
18 LIRIC coarse mode is comprised only of non-spherical particles. Figure 6b shows the
19 comparison of GARRLiC and LIRIC dust particle profiles with the BSC DREAM8b model. For
20 this comparison we consider all particles in GARRLiC and LIRIC profiles to be dust particles.
21 Furthermore, we multiply them with the dust density of 2.6 g cm^{-3} (Reid et al., 2003) to convert
22 the volume concentration ratio (in ppb) to dust mass concentration (in $\mu\text{g m}^{-3}$). Although the
23 shapes agree well, the BSC DREAM8b model values are lower than GARRLiC and LIRIC, by
24 a factor of 2. The BSC DREAM8b underestimation when comparing to LIRIC is consistent with
25 the findings of Biniotoglou et al. (2015) for relative low dust concentrations (as is the case here).
26 The underestimation is shown in the BSC DREAM8b dust AOD at 550 nm as well, with a value
27 of ~ 0.2 , which is half of the sun-photometer-measured AOD at 500 nm, of 0.4. When we scale
28 the BSC-DREAM8b concentration with these AOD values (multiplying by a factor of 2) the
29 bias is reduced to less than 10% at 1 km and 50% at 3 km, relative to GARRLiC and LIRIC
30 concentrations. The GARRLiC and LIRIC mass concentrations are compared also with surface
31 in situ PM_{10} measurements, showing the algorithms overestimating the particle concentration at
32 the surface level (Fig. 6c). We calculate the PM_{10} concentrations from GARRLiC and LIRIC

1 mass concentrations, as percentages of the particles with diameter less than 10 μm (i.e., 83%
2 and 80% of the total mass, respectively). Figure 6c shows the GARRLiC and LIRIC PM_{10}
3 surface values (purple stars in plot), considering marine instead of dust particles at the surface,
4 thus using the marine particle density for the volume to mass conversion (i.e., 1.7 g cm^{-3} for
5 dry marine particles (Stock et al., 2011), since the measured RH at the surface is 16%). The
6 agreement with the surface in situ measurements is better now, but it is only indicative, since
7 what we have at the surface is most probably a mixture of marine, continental and dust particles
8 as shown in Fig 3b.

9 Summarizing, the GARRLiC and LIRIC retrievals are performing well for the dust episode on
10 July 26, considering the consistency with the Klett retrievals, the BSC DREAM8b modelled
11 mass concentration profiles, the surface in situ measurements of the fine mode size distribution,
12 as well as the expected increase of the dust absorption in the ultraviolet. The discrepancies seen
13 for the retrieval closer to the surface and the PM_{10} at the surface level can be explained if we
14 consider the incomplete lidar information in the overlap region.

15 **3.2 Marine and polluted continental particle case**

16 On July 15 the lidar measurements at 12:30-14:30 UTC showed a low-AOD layer of non-
17 depolarizing particles, extending up to 3 km (Fig. 7a). The lack of depolarization indicates
18 spherical (hydrated) marine particles which is also supported by our source-receptor analysis
19 (Fig. 7b). Specifically, FLEXPART-WRF simulations show that the particles above Finokalia
20 station have mainly a marine origin along the whole atmospheric column, with a possible
21 contribution of continental aerosol from Southern Italy. This scenario is further supported by
22 AERONET measurements at 13:24 UTC, of low AOD of ~ 0.06 at 500 nm, high Ångström
23 exponent of ~ 1.2 at 440/870 nm and low refractive index of $\sim 1.4+i0.0005$ at 440 nm, which are
24 within the climatological value ranges for marine particles and their mixtures, as reported from
25 Dubovik et al. (2002).

26 The low AOD is unfavourable for the GARRLiC and AERONET microphysical property
27 retrievals, especially for the spectral refractive index and SSA (Dubovik et al., 2000b; Lopatin
28 et al., 2013). The latter require an AOD of at least 0.4 at 440 nm for satisfactory accuracy in
29 case of sun-photometer-only retrieval (Dubovik et al., 2000b). The lidar information combined
30 with the sun-photometer measurements in GARRLiC is expected to improve the retrieval in
31 low AOD cases (Lopatin et al., 2013). Although the AOD requirements have not been

1 quantified yet for GARRLiC, an AOD of 0.3 at 440 nm is considered sufficient. As reported
2 in Dubovik et al. (2002) though, the marine particles rarely exceed the AOD of 0.15 at 440 nm,
3 thus we do not expect highly accurate refractive index and SSA retrievals from GARRLiC, or
4 from AERONET/LIRIC, for the marine particles. Even more so, the marine case analysed here
5 has a much lower AOD, thus we consider the refractive index and SSA retrievals to be only
6 indicative for this case. In addition, as seen in Fig. 7a, most of the aerosol load is located below
7 1 km, where the lidar incomplete overlap region is located, which challenges even more the
8 combined lidar/sun-photometer retrieval.

9 The GARRLiC and LIRIC retrievals used the lidar measurements at 12:30-14:30 UTC (red box
10 in Fig. 7a) and the sun-photometer measurements at 13:24 UTC. Figure 8 shows the retrieved
11 backscatter and extinction coefficients at 355, 532 and 1064 nm, and the corresponding
12 retrievals from the Klett method. For the latter we consider LRs of 50, 45 and 45 sr for 355,
13 532 and 1064, respectively, that closely reproduce the sun-photometer measured AODs of 0.1,
14 0.05 and 0.02 at 340, 500 and 1020 nm. The agreement between GARRLiC and LIRIC is
15 satisfactory within the LIRIC uncertainties (Fig. 8a and b). Above 550 m, this is also the case
16 for GARRLiC and Klett backscatter coefficient retrievals, whereas for the extinction
17 coefficients the differences are within 30% for 355 nm and 10-40% for 532 nm relative to
18 GARRLiC values (Fig. 8c and d). In the marine boundary layer (below 550 m) the Klett NF
19 backscatter and extinction coefficients at 532 nm show much larger values than the ones
20 retrieved from GARRLiC and LIRIC. This highlights very vividly the importance of the NF
21 measurements in properly retrieving the marine particle properties with lidars.

22 GARRLiC retrieves both fine and coarse particles in this case, which we consider to be mainly
23 of continental and marine origin, respectively. The fine particle volume size distribution shows
24 ~10% more volume than the AERONET product and the surface in situ SMPS measurements
25 (Fig. 9, up left). The SMPS volume size distribution is converted to $\mu\text{m}^3\mu\text{m}^{-2}$ considering that
26 most particles reside from the surface up to ~ 1 km (Fig. 7). The difference may be partly due
27 to the instrument drying the particle sample, but the effect is not expected to be that strong since
28 the RH at the surface is 60% and the corresponding hygroscopic growth is estimated at 1.17
29 (section 2.1.3, Eq. 2). For the coarse mode, GARRLiC retrieves ~50% more volume than
30 AERONET. The AERONET SSA and spectral refractive index retrievals are the same with the
31 GARRLiC fine mode retrievals, or within the retrieval uncertainty (Fig. 9). These high values
32 of SSA (close to 1) and the refractive index of $1.38\pm 0.4+i0.0005\pm 0.0003$ are within the range

1 of climatological values of continental particles, according to Dubovik et al. (2002). For the
2 GARRLiC coarse mode, the SSA and imaginary part of the refractive index show very high
3 values for marine particles, which are most probably false, whereas the real part of the refractive
4 index of ~ 1.36 agrees well with the climatological value of 1.36 ± 0.01 for marine particles
5 (Dubovik et al., 2002).

6 Figure 10a shows the GARRLiC and LIRIC volume concentration profiles, which agree well
7 within the LIRIC retrieval uncertainties above 550 m, whereas below the GARRLiC
8 concentration for the coarse particles is larger. Assuming that the marine particles are comprised
9 only of coarse particles, we derive the marine mass concentration profiles from GARRLiC and
10 LIRIC as shown in Fig. 10b. The mass concentration profiles are calculated from the coarse
11 volume concentration profiles using a sea salt density of 1.3 g cm^{-3} . This value denotes the
12 density of a sea salt solution at a RH of 50-60 % (Eq. 3 in Zhang et al. (2005)), with the RH
13 values provided from the RAMS model. Figure 10b shows also the RAMS-ICLAMS sea salt
14 model mass concentration profile which presents lower values than GARRLiC and LIRIC, with
15 differences of $\sim 80\%$ and 60% at the surface, respectively. Moreover, GARRLiC and LIRIC
16 PM_{10} mass concentrations seem to agree well with the surface in situ PM_{10} measurements (Fig.
17 10c) within the time variability of the latter. The GARRLiC and LIRIC PM_{10} values are
18 calculated using the respective percentages of volume size distributions for particles with
19 diameter less than $10 \mu\text{m}$ (i.e., the sum of fine mode volume and 35% of coarse mode volume
20 for GARRLiC and 50% of total volume for AERONET/LIRIC). The comparison with the in
21 situ measurements should also consider the drying of the ambient sample by the in situ
22 instrument. We calculate the GARRLiC and LIRIC “dry” PM_{10} , considering a hygroscopic
23 growth factor of 1.17 at $\text{RH}=60\%$ at the surface (section 2.1.3). The “dry” values agree well
24 with the in situ measurements, within the latter time variability.

25 Summarizing, GARRLiC retrieves more fine particles than AERONET and surface in situ
26 measurements. The fine particle SSA and refractive index is characteristic of continental
27 particles. The corresponding coarse mode retrieval probably fails for SSA and the imaginary
28 part of the refractive index, which are very difficult to be retrieved with low AODs, but the real
29 part of the refractive index properly assigns the refractive index of marine particles. Both
30 GARRLiC and LIRIC concentration profiles seem to agree well with the PM_{10} surface in situ
31 measurements. Since the marine-dominated scenes usually have very low AOD and low vertical
32 extent (Ho et al., 2015), it is challenging to obtain trustworthy retrievals from GARRLiC and

1 LIRIC for marine particle scenes. One way to improve the marine retrievals in future efforts is
2 to try to increase the lidar information in the overlap region, utilizing for example the NF lidar
3 measurements, as discussed in section 3.1.1.

4 **3.3 Dust and marine case**

5 On July 4 a mixture of dust, marine and continental aerosols was observed at Finokalia station.
6 Figure 11a, shows at 4-6 UTC an advected depolarizing dust plume at 4-6 km and a less-
7 depolarizing plume extending from the ground up to 2-3 km, with volume depolarization ratios
8 at 532 nm of 0.1 and <0.05 , respectively. This is a weak dust episode, with a measured column
9 AOD of ~ 0.15 at 500 nm, which according to the AERONET and GARRLiC uncertainty
10 standards discussed in Section 4.2 should not be sufficient for a full characterization of the
11 particles. The dust and marine particle transport is supported by the BSC DREAM8b dust model
12 and RAMS-ICLAMS sea salt model simulations (Fig. 12b), respectively, as well as from our
13 FLEXPART-WRF source-receptor calculations (Fig. 11b). The latter show mainly Saharan
14 dust particles at 4-6 km, marine particles mostly from the Aegean Sea along with continental
15 particles from the Balkans up to 1 km, and a mixture of marine, continental and dust particles
16 at 1-3 km.

17 GARRLiC retrieves these three layers (Fig. 12a) but it cannot characterize them effectively in
18 terms of their refractive indices, since it is able to retrieve only one refractive index for each
19 mode. For example, the coarse mode of the dust/marine mixture contains dust particles with a
20 real part of refractive index of $\sim 1.55-1.65$ (e.g. Kandler et al., 2007) together with marine
21 particles of quite different refractive index, with a real part of ~ 1.35 (Dubovik et al., 2002).
22 Thus, what we get from GARRLiC as the refractive index of the mixture coarse mode is
23 possibly closer to an average of the refractive indices of dust and marine particles. This is shown
24 in Fig. 13 (down, right), with the GARRLiC coarse mode refractive index to have a value of
25 1.45 for the real part. The imaginary part of the coarse mode and the SSA show an unusual
26 increase and decrease, respectively, towards the longer wavelengths, which is most probably
27 false. The fine mode should contain mostly continental particles, but the retrieved refractive
28 index of $1.36+i0.001$ is more characteristic for marine particles (Dubovik et al., 2002). The
29 AERONET retrieval (used in LIRIC algorithm) assigns a marine refractive index
30 ($\sim 1.35+i0.0005$) to both fine and coarse particles. The fine mode size distribution compares
31 well with AERONET, but presents slightly lower values than SMPS surface in situ

1 measurements (Fig. 13, up left). With a surface RH of 75%, corresponding to a hygroscopic
2 growth factor of 1.3 (Eq. 2), the GARRLiC fine particle size distribution should be larger than
3 the SMPS dried particle measurements.

4 Figure 14 shows the potential of GARRLiC to retrieve the “marine” and “dust” components of
5 the mixture, by changing the definition of the two modes retrieved: instead of “fine” and
6 “coarse” mode GARRLiC is set to retrieve two modes that span the whole size range so as both
7 contain coarse particles, and it derives a “dust” mode that contains only coarse particles and a
8 “marine” mode that contains both fine and coarse particles, of bigger size than “dust”. Raptis
9 et al. (2015) showed similar results for the marine and dust size distribution using their
10 multimodal analysis for a different dust/marine mixture case during the CHARADMExp
11 campaign. The retrieved real part of the refractive index is ~ 1.33 for “marine” particles and
12 ~ 1.47 for “dust” particles. Although these values are very close to the climatological values for
13 marine and dust particles, the retrievals of the imaginary part of the refractive index and the
14 volume concentration profiles are not satisfactory (not shown here). We believe that these
15 results show a potential for successful marine/dust mixture characterization from GARRLiC in
16 the future, if the new versions of the algorithm utilize the cross-polarized signals as well. As in
17 LIRIC, the polarization measurements will help to derive the spherical (marine) and non-
18 spherical (dust) components of the mixture.

19 LIRIC provides the dust and marine vertical distribution, since it disentangles the coarse particle
20 volume concentration profile to its spherical (marine) and non-spherical (dust) components
21 (Fig. 12a, right). Assuming a very low contribution from dust and marine particles in the fine
22 mode we acquire the “marine” and “dust” concentration profiles from the spherical and non-
23 spherical coarse particle concentration profiles, respectively. Figure 12b shows that LIRIC
24 marine and dust mass concentration profiles have larger values than the BSC DREAM8b dust
25 and the RAMS-ICLAMS sea salt models, respectively. In order to acquire the mass
26 concentration profiles, LIRIC dust and marine volume profiles are multiplied with the density
27 values of 2.6 g cm^{-3} (Reid et al., 2003) and 1.25 g cm^{-3} , respectively. The marine particle
28 density corresponds to 60-80% RH (Zhang et al., 2005), as this is provided by the RAMS model
29 at 0-1 km. We believe that BSC DREAM8b model underestimates the dust concentration, as
30 for the dust case in section 4.1, since the model AOD of ~ 0.025 at 500 nm is approximately 5
31 times lower than the sun-photometer measured AOD at 550 nm (not taking into account the
32 AOD contribution of the marine and continental particles). Multiplying the BSC DREAM8b

1 dust profile by 5 we get a better agreement with LIRIC dust profile at 4-6 km, but in the mixed
2 layer at 0-3 km this agreement is not satisfactory (not shown here). The RAMS-ICLAMS model
3 show lower sea salt concentration than LIRIC (as in section 4.2), with ~60 % differences at the
4 surface level. Figure 12c shows that LIRIC PM_{10} values agree well with the surface in situ
5 measurements, within the latter time variability. The LIRIC PM_{10} is calculated using the volume
6 percentage of the particles with diameter less than 10 μm (i.e., 60% of the total volume).
7 Moreover, we calculate the LIRIC “dry” PM_{10} using Eq.1 and considering a particle
8 hygroscopic growth of 1.3 for $RH=75\%$ at the surface (Eq.2). The LIRIC “dry” PM_{10} is lower
9 than the surface in situ measurements, at ~50% of their mean value. For GARRLiC the PM_{10}
10 profile cannot be calculated, since the corresponding volume concentration profile is a mixture
11 of dust, marine and continental particles with unknown density.

12 Figure 15 shows the backscatter and extinction coefficients retrieved with GARRLiC, LIRIC
13 and Klett methods. GARRLiC and LIRIC agree well within the LIRIC uncertainties (Fig. 15a
14 and b). The agreement with Klett retrievals is satisfactory for the backscatter coefficient at 532
15 and 1064 nm above 550 m, within their uncertainties, with 60-130% differences seen for the
16 355 nm retrieval (Fig. 15c). As for the marine case in section 4.2, the NF backscatter coefficient
17 at 532 nm show much larger values. The same holds for the NF extinction coefficient at 532
18 nm (Fig. 15d). The Klett extinction coefficients at 1-3 km are up to 60% and 50% lower than
19 GARRLiC at 355 and 532 nm, respectively.

20 Overall, this is a challenging case for both GARRLiC and LIRIC algorithms. We can claim that
21 GARRLiC shows some potential in providing a successful dust and marine microphysical
22 property characterization in case more information (e.g. cross-polarized lidar signal) is included
23 in the retrieval. Moreover, the LIRIC capability of providing the vertical distribution of dust
24 and marine particles is mostly successful, comparing the results with our source-receptor
25 simulations and the surface in situ PM_{10} measurements. As is the case also for the marine
26 particle characterization in section 4.2, we believe that this retrieval will be greatly benefited
27 from NF measurements.

28

29 **4 Summary and Conclusions**

30 GARRLiC and LIRIC algorithms provide the great innovation of retrieving the vertical
31 distribution of aerosol microphysics utilizing the synergy of the elastic backscatter lidar and

1 sun-photometer techniques. This way the algorithms show the potential to effectively
2 characterize the vertical distribution of fine, coarse spherical and coarse non-spherical particle
3 concentrations in the case of LIRIC, and the concentration profiles of fine and coarse particles,
4 along with their column-averaged size, shape and spectral refractive index, in case of
5 GARRLiC.

6 In this study we used both algorithms to characterize three cases of dust and marine presence
7 during the ESA-CHARADMExp experimental campaign. For the first case GARRLiC achieves
8 a successful retrieval of the dust vertical distribution and microphysical characterization that
9 agrees well with AERONET and climatological values for dust, within the respective
10 uncertainties. Both LIRIC and GARRLiC concentration profiles are found to be consistent with
11 the BSC DREAM8b dust vertical structure, showing though up to 100% larger values than the
12 surface in situ PM_{10} measurements. For the second case consisting of mainly marine particles,
13 both algorithms provide satisfactory concentration retrievals, well within the time variability of
14 the surface in situ PM_{10} measurements. The GARRLiC microphysical property retrieval is
15 mostly not successful for the marine particles, with e.g. ~10% more fine particle volume than
16 the AERONET product and the surface in situ measurements. This is due to the difficulties
17 posed by the really low AOD and the insufficient lidar information in the overlap region, where
18 most of the marine aerosol load resides. Last, for the more challenging case of dust and marine
19 mixture, LIRIC provides the dust and marine particle vertical structure due to its capability to
20 retrieve the coarse mode spherical (marine) and non-spherical (dust) components. GARRLiC
21 shows potential in disentangling the marine and dust components, if more information is
22 included in the algorithm input.

23 The difficulties posed in retrieving the concentration profiles and the microphysical properties
24 of dust and marine particle mixtures in the atmospheric column have to do with the low AOD
25 of the marine plumes, the insufficient lidar information in the overlap region and the number of
26 modes considered from the retrievals. For GARRLiC, the retrieval of multiple modes would be
27 possibly feasible in the future with the incorporation of polarimetric measurements from the
28 sun-photometer and/or the cross-polarized and Raman signals from the lidar. Moreover, we
29 could try to increase the near-surface information from the lidar, performing the signal gluing
30 technique between the FF and NF measurements and/or by using additional information
31 available from in situ observations. We aim to continue investigating the GARRLiC and LIRIC

1 potential for aerosol characterization and follow related improvements in the framework of the
2 ACTRIS-2 project and the experimental campaigns that are dedicated to that objective.

3

4

5

6 **Acknowledgements**

7 The research leading to these results has received funding from the European Union’s Horizon
8 2020 Research and Innovation Programme ACTRIS-2 (grant agreement no. 654109). The work
9 has been developed under the auspices of the ESA-ESTEC project “Characterization of Aerosol
10 mixtures of Dust And Marine origin” contract no. IPL-PSO/FF/1f/14.489. The publication was
11 supported by the European Union’s Horizon 2020 Research and Innovation programme under
12 grant agreement No 602014, project ECARS (East European Centre for Atmospheric Remote
13 Sensing). BSC-DREAM8b simulations were performed on the Mare Nostrum supercomputer
14 hosted by the Barcelona Supercomputing Center–Centro Nacional de Supercomputación
15 (BSC).

16

1 **References**

- 2 Althausen, D., Engelmann, R., Baars, H., Heese, B., Ansmann, A., Mueller, D., and Komppula,
3 M.: Portable Raman lidar PollyXT for automated profiling of aerosol backscatter, extinction,
4 and depolarization, *Journal of Atmospheric and Oceanic Technology*, 26, 2366–2378,
5 10.1175/2009JTECHA1304.1, 2009.
- 6 Amiridis, V., Kafatos, M., Pérez, C., Kazadzis, S., Gerasopoulos, E., Mamouri, R. E.,
7 Papayannis, A., Kokkalis, P., Giannakaki, E., Basart, S., Daglis, I., and Zerefos, C.: The
8 potential of the synergistic use of passive and active remote sensing measurements for the
9 validation of a regional dust model, *Ann. Geophys.*, 27, 3155–3164, doi:10.5194/angeo-27-
10 3155-2009, 2009.
- 11 Amiridis, V., Wandinger, U., Marinou, E., Giannakaki, E., Tsekleri, A., Basart, S., Kazadzis,
12 S., Gkikas, A., Taylor, M., Baldasano, J., and Ansmann, A.: Optimizing Saharan dust
13 CALIPSO retrievals, *Atmos. Chem. Phys. Discuss.*, 13, 14749–14795, doi:10.5194/acpd-13-
14 14749-2013, 2013.
- 15 Ansmann, A., Riebesell, M., and Weitkamp, C.: Measurement of atmospheric aerosol
16 extinction profiles with a Raman lidar, *Opt. Lett.*, 15, 746-748, 1990.
- 17 Ansmann, A., Tesche, M., Seifert, P., Groß, S., Freudenthaler, V., Apituley, A., Wilson, K. M.,
18 Serikov, I., Linné, H., Heinold, B., Hiebsch, A., Schnell, F., Schmidt, J., Mattis, I., Wandinger,
19 U., and Wiegner, M.: Ash and fine-mode particle mass profiles from EARLINET-AERONET
20 observations over central Europe after the eruptions of the Eyjafjallajökull volcano in 2010, *J.*
21 *Geophys. Res. Atmospheres*, 116(D20), D00U02, doi:10.1029/2010JD015567, 2011.
- 22 Ansmann, A., Seifert, P., Tesche, M., and Wandinger, U.: Profiling of fine and coarse particle
23 mass: case studies of Saharan dust and Eyjafjallajökull/Grimsvötn volcanic plumes, *Atmos*
24 *Chem Phys*, 12(20), 9399–9415, doi:10.5194/acp-12-9399-2012, 2012.
- 25 Baars, H., Kanitz, T., Engelmann, R., Althausen, D., Heese, B., Komppula, M., Preißler, J.,
26 Tesche, M., Ansmann, A., Wandinger, U., Lim, J.-H., Ahn, J. Y., Stachlewska, I. S., Amiridis,
27 V., Marinou, E., Seifert, P., Hofer, J., Skupin, A., Schneider, F., Bohlmann, S., Foth, A., Bley,
28 S., Pfüller, A., Giannakaki, E., Lihavainen, H., Viisanen, Y., Hooda, R. K., Pereira, S. N.,
29 Bortoli, D., Wagner, F., Mattis, I., Janicka, L., Markowicz, K. M., Achtert, P., Artaxo, P.,
30 Pauliquevis, T., Souza, R. A. F., Sharma, V. P., van Zyl, P. G., Beukes, J. P., Sun, J., Rohwer,
31 E. G., Deng, R., Mamouri, R.-E., and Zamorano, F.: An overview of the first decade of Polly^{NET}:

1 an emerging network of automated Raman-polarization lidars for continuous aerosol profiling,
2 *Atmos. Chem. Phys.*, 16, 5111-5137, doi:10.5194/acp-16-5111-2016, 2016.

3 Babin, M., Morel, A., Fournier-Sicre, V., Fell, F., Stramski, D.: Light scattering properties of
4 marine particles in coastal and open ocean waters as related to the particle mass concentration,
5 *Limnology and Oceanography*, 2, doi: 10.4319/lo.2003.48.2.0843, 2003.

6 Balis, D., Amiridis, V., Nickovic, S., Papayannis, A., and Zerefos, C.: Optical properties of
7 Saharan dust layers as detected by a Raman lidar at Thessaloniki, Greece, *Geophysical*
8 *Research Letters*, 31, L13104, doi:10.1029/2004GL019881, 2004.

9 Basart, S., Pérez García-Pando, C., Cuevas, E., Baldasano Recio, J. M., and Gobbi, P.: Aerosol
10 characterization in Northern Africa, Northeastern Atlantic, Mediterranean basin and Middle
11 East from direct-sun AERONET observations, *Atmospheric Chemistry and Physics*, 9(21),
12 8265-8282, 2009.

13 Basart, S., Pérez, C., Nickovic, S., Cuevas, E., and Baldasano, J. M.: Development and
14 evaluation of the BSC-DREAM8b dust regional model over Northern Africa, the
15 Mediterranean and the Middle East, *Tellus B*, 64, 18539, doi:10.3402/tellusb.v64i0.18539,
16 2012a.

17 Basart, S., Pay, M. T., Jorba, O., Pérez, C., Jiménez-Guerrero, P., Schulz, M., and Baldasano,
18 J. M.: Aerosols in the CALIOPE air quality modelling system: evaluation and analysis of PM
19 levels, optical depths and chemical composition over Europe, *Atmos. Chem. Phys.*, 12, 3363–
20 3392, doi:10.5194/acp-12-3363-2012, 2012b.

21 Biniatoglou, I., Basart, S., Alados-Arboledas, L., Amiridis, V., Argyrouli, A., Baars, H.,
22 Baldasano, J. M., Balis, D., Belegante, L., Bravo-Aranda, J. A., Burlizzi, P., Carrasco, V.,
23 Chaikovsky, A., Comerón, A., D'Amico, G., Filioglou, M., Granados-Muñoz, M. J., Guerrero-
24 Rascado, J. L., Ilic, L., Kokkalis, P., Maurizi, A., Mona, L., Monti, F., Muñoz-Porcar, C.,
25 Nicolae, D., Papayannis, A., Pappalardo, G., Pejanovic, G., Pereira, S. N., Perrone, M. R.,
26 Pietruczuk, A., Posyniak, M., Rocadenbosch, F., Rodríguez-Gómez, A., Sicard, M., Siomos, N.,
27 Szkop, A., Terradellas, E., Tsekeri, A., Vukovic, A., Wandinger, U., and Wagner, J.: A
28 methodology for investigating dust model performance using synergistic
29 EARLINET/AERONET dust concentration retrievals, *Atmos. Meas. Tech.*, 8, 3577-3600,
30 doi:10.5194/amt-8-3577-2015, 2015.

1 Bezantakos, S., Barmounis, K., Giamarelou, M., Bossioli, E., Tombrou, M., Mihalopoulos, N.,
2 Eleftheriadis, K., Kalogiros, J., D. Allan, J., Bacak, A., Percival, C. J., Coe, H., and Biskos, G.:
3 Chemical composition and hygroscopic properties of aerosol particles over the Aegean Sea,
4 *Atmos. Chem. Phys.*, 13, 11595-11608, doi:10.5194/acp-13-11595-2013, 2013.

5 Bovchaliuk, V., Goloub, P., Podvin, T., Veselovskii, I., Tanre, D., Chaikovsky, A., Dubovik,
6 O., Mortier, A., Lopatin, A., Korenskiy, M., and Victori, S.: Comparison of aerosol properties
7 retrieved using GARRLiC, LIRIC, and Raman algorithms applied to multi-wavelength LIDAR
8 and sun/sky-photometer data, *Atmos. Meas. Tech. Discuss.*, doi:10.5194/amt-2016-40, in
9 review, 2016.

10 Brioude, J., Arnold, D., Stohl, A., Cassiani, M., Morton, D., Seibert, P., Angevine, W., Evan,
11 S., Dingwell, A., Fast, J. D., Easter, R. C., Pisso, I., Burkhardt, J., and Wotawa, G.: The
12 Lagrangian particle dispersion model FLEXPART-WRF version 3.1, *Geosci. Model Dev.*, 6,
13 1889-1904, doi:10.5194/gmd-6-1889-2013, 2013.

14 Chaikovsky, A., Dubovik, O., Holben, B., Bril, A., Goloub, P., Tanré, D., Pappalardo, G.,
15 Wandinger, U., Chaikovskaya, L., Denisov, S., Grudo, J., Lopatin, A., Karol, Y., Lapyonok, T.,
16 Amiridis, V., Ansmann, A., Apituley, A., Allados-Arboledas, L., Biniotoglou, I., Boselli, A.,
17 D'Amico, G., Freudenthaler, V., Giles, D., Granados-Muñoz, M. J., Kokkalis, P., Nicolae, D.,
18 Oshchepkov, S., Papayannis, A., Perrone, M. R., Pietruczuk, A., Rocadenbosch, F., Sicard, M.,
19 Slutsker, I., Talianu, C., De Tomasi, F., Tsekeri, A., Wagner, J., and Wang, X.: Lidar-
20 Radiometer Inversion Code (LIRIC) for the retrieval of vertical aerosol properties from
21 combined lidar/radiometer data: development and distribution in EARLINET, *Atmos. Meas.*
22 *Tech.*, 9, 1181-1205, doi:10.5194/amt-9-1181-2016, 2016.

23 Cotton, W. R., Pielke, Sr., R. A., Walko, R. L., Liston, G. E., Tremback, C. J., Jiang, H.,
24 McAnelly, R. L., Harrington, J. Y., Nicholls, M. E., Carrio, G. G., and Mc Fadden, J. P.:
25 RAMS 2001: Current status and future directions, *Meteorol. Atmos. Phys.*, 82, 5–29, 2003.

26 Dubovik, O. and King, M: A flexible inversion algorithm for retrieval of aerosol optical
27 properties from Sun and sky radiance measurements, *J. Geophys. Res.*, 105, 20673–20696,
28 doi:10.1029/2000JD900282, 2000a.

29 Dubovik, O., Smirnov, A., Holben, B. N., King, M. D., Y. J. Kaufman, Eck, T. F., and Slutsker,
30 I.: Accuracy assessment of aerosol optical properties retrieval from AERONET sun and sky
31 radiance measurements, *J. Geophys. Res.*, 105, 9791–9806, 2000b.

1 Dubovik, O., Holben, B., Eck, T., Smirnov, A., Kaufman, Y., King, M., Tanré, D., and Slutsker,
2 I.: Variability of absorption and optical properties of key aerosol types observed in worldwide
3 locations, *J. Atmos. Sci.*, 59, 590–608, 2002.

4 Dubovik, O.: Optimization of Numerical Inversion in Photopolarimetric Remote Sensing, in:
5 Photopolarimetry in Remote Sensing, edited by: Videen, G., Yatskiv, Y., and Mishchenko, M.,
6 Kluwer Academic Publishers, Dordrecht, the Netherlands, 65–106, 2004.

7 Dubovik, O., Sinyuk, A., Lapyonok, T., Holben, B. N., Mishchenko, M., Yang, P., Eck, T.F.,
8 Volten, H., Muñoz, O., Veihelmann, B., van der Zande, W. J., Leon, J. -F., Sorokin, M., and
9 Slutsker, I.: Application of spheroid models to account for aerosol particle nonsphericity in
10 remote sensing of desert dust, *J. Geophys. Res.*, 111, D11208, doi:10.1029/2005JD006619,
11 2006.

12 Dubovik, O., Lapyonok, T., Litvinov, P., Herman, M., Fuertes, D., Ducos, F., Lopatin, A.,
13 Chaikovsky, A., Torres, B., Derimian, Y., Huang, X., Aspetsberger, M., and Federspiel, C.:
14 GRASP: a versatile algorithm for characterizing the atmosphere, *SPIE: Newsroom*, Sep., 2014.

15 Engelmann, R., Kanitz, T., Baars, H., Heese, B., Althausen, D., Skupin, A., Wandinger, U.,
16 Komppula, M., Stachlewska, I. S., Amiridis, V., Marinou, E., Mattis, I., Linné, H., and
17 Ansmann, A.: The automated multiwavelength Raman polarization and water-vapor lidar
18 Polly^{XT}: the neXT generation, *Atmos. Meas. Tech.*, 9, 1767-1784, doi:10.5194/amt-9-1767-
19 2016, 2016.

20 Fernald, F. G., Herman, B. M., and Reagan, J. A.: Determination of aerosol height distributions
21 by lidar, *J. Appl. Meteorol.*, 11, 482–489, 1972.

22 Gerasopoulos E., Kouvarakis G., Babasakalis P., Vrekoussis M., Putaud J.P., and Mihalopoulos
23 N.: Origin and variability of particulate matter (PM10) mass concentrations over the Eastern
24 Mediterranean, *Atmos. Environ.*, 40, 4679-4690, 2006.

25 Gobbi, G. P., Angelini, F., Barnaba, F., Costabile, F., Baldasano, J. M., Basart, S., and
26 Bolignano, A.: Changes in particulate matter physical properties during Saharan advections
27 over Rome (Italy): a four-year study, 2001–2004. *Atmospheric Chemistry and Physics*, 13(15),
28 7395-7404, 2013.

29 Gong, S. L., Barrie, L. A., and Lazare, M.: Canadian Aerosol Module (CAM): a size-segregated
30 simulation of atmospheric aerosol processes for climate and air quality models. 2. Global

1 sea-salt aerosol and its budgets, *J. Geophys. Res.*, 107(D24), 4779, doi:10.1029/2001JD002004,
2 2002.

3 Granados-Muñoz, M. J., Guerrero-Rascado, J. L., Bravo-Aranda, J. A., Navas-Guzmán, F.,
4 Valenzuela, A., Lyamani, H., Chaikovsky, A., Wandinger, U., Ansmann, A., Dubovik, O.,
5 Grudo, J., and Alados-Arboledas, L.: Retrieving aerosol microphysical properties by Lidar-
6 Radiometer Inversion Code (LIRIC) for different aerosol types, *J. Geophys. Res.*, 119,
7 4836–4858, doi:10.1002/2013JD021116, 2014.

8 Granados-Muñoz, M. J., Bravo-Aranda, J. A., Baumgardner, D., Guerrero-Rascado, J. L.,
9 Pérez-Ramírez, D., Navas-Guzmán, F., Veselovskii, I., Lyamani, H., Valenzuela, A., Olmo, F.
10 J., Titos, G., Andrey, J., Chaikovsky, A., Dubovik, O., Gil-Ojeda, M., and Alados-Arboledas,
11 L.: Study of aerosol microphysical properties profiles retrieved from ground-based remote
12 sensing and aircraft in-situ measurements during a Saharan dust event, *Atmos. Meas. Tech.*
13 *Discuss.*, 8, 9289–9338, doi:10.5194/amtd-8-9289-2015, 2015.

14 Granados-Muñoz, M. J., Navas-Guzmán, F., Guerrero-Rascado, J. L., Bravo-Aranda, J. A.,
15 Biniotoglou, I., Pereira, S. N., Basart, S., Baldasano, J. M., Belegante, L., Chaikovsky, A.,
16 Comerón, A., D'Amico, G., Dubovik, O., Ilic, L., Kokkalis, P., Muñoz-Porcar, C., Nickovic, S.,
17 Nicolae, D., Olmo, F. J., Papayannis, A., Pappalardo, G., Rodríguez, A., Schepanski, K., Sicard,
18 M., Vukovic, A., Wandinger, U., Dulac, F., and Alados-Arboledas, L.: Profiling of aerosol
19 microphysical properties at several EARLINET/AERONET sites during the July 2012
20 ChArMEx/EMEP campaign, *Atmos. Chem. Phys.*, 16, 7043-7066, doi:10.5194/acp-16-7043-
21 2016, 2016.

22 Haustein, K., Pérez, C., Baldasano, J. M., Müller, D., Tesche, M., Schladitz, A., Freudenthaler,
23 V., Heese, B., Esselborn, M., Weinzierl, B., Kandler, K., and von Hoyningen-Huene, W.:
24 Regional dust model performance during SAMUM 2006, *Geophys. Res. Lett.*, 36, L03812,
25 doi:10.1029/2008GL036463, 2009.

26 Ho, S. -p., Peng, L., Anthes, R. A., Kuo, Y. -H., and Lin, H. -C.: Marine Boundary Layer Heights
27 and Their Longitudinal, Diurnal, and Interseasonal Variability in the Southeastern Pacific Using
28 COSMIC, CALIOP, and Radiosonde Data, *Journal of Climate*, 28, 2856, 2015.

29 Holben, B. N., Eck, T. F., Slutsker, I., Tanre, D., Buis, J. P., Setzer, A., Vermote, E., Reagan,
30 J. A., Kaufman, Y. J., Nakajima, T., Lavenu, F., Jankowiak, I., and Smirnov, A.: AERONET-

1 A federated instrument network and data archive for aerosol characterization, *Remote Sens.*
2 *Environ.*, 66(1), 1–16, doi:10.1016/S0034-4257(98)00031-5, 1998.

3 Jiménez-Guerrero, P., Pérez, C., Jorba, O., and Baldasano, J. M.: Contribution of Saharan dust
4 in an integrated air quality system and its on-line assessment, *Geophys. Res. Lett.*, 35, L03814,
5 doi:10.1029/2007GL031580, 2008.

6 Kalivitis, N., Gerasopoulos, E., Vrekoussis, M., Kouvarakis, G., Kubilay, N., Hatzianastassiou,
7 N., Vardavas, I., and Mihalopoulos, N.: Dust transport over the eastern Mediterranean derived
8 from Total Ozone Mapping Spectrometer, Aerosol Robotic Network, and surface
9 measurements, *J. Geophys. Res.*, 112, D03202, doi:10.1029/2006JD007510, 2007.

10 Klett, D.: Lidar inversion with variable backscatter/extinction ratios, *Appl. Optics*, 31, 1638–
11 1643, 1985.

12 Kokkalis, P., Amiridis, V., Allan, J. D., Papayannis, A., Solomos, S., Tsekeri, A., Rosenberg,
13 P. D., Biniotoglou, I., Marinou, E., Vasilescu, J., Nicolae, D., Coe, H., Bacak, A., Chaikovsky,
14 A.: Validation of LIRIC aerosol concentration retrievals using airborne measurements over
15 Athens, submitted in *Atmospheric Research*, 2016.

16 Lawrence, M.G.: The relationship between relative humidity and the dewpoint temperature in
17 moist air: a simple conversion and applications, *Bull. Am. Meteorol. Soc.*, 86, 225–233, 2005,
18 <http://dx.doi.org/10.1175/BAMS-86-2-225>.

19 Leeuw, G., Neele, F. P., Hill, M., Smith, M. H., and Vignali, E.: Production of sea spray aerosol
20 in the surf zone, *J. Geophys. Res. Atmos.*, 105, 29397–29409, 2000.

21 Lelieveld, J., Berresheim, H., Borrmann, S., Crutzen, P., Dentener, F., Fischer, H., Feichter, J.,
22 Flatau, P., Heland, J., Holzinger, R., Korrman, R., Lawrence, M., Levin, Z., Markowicz, K.,
23 Mihalopoulos, N., Minikin, A., Ramanathan, V., de Reus, M., Roelofs, G., Scheeren, H., Sciare,
24 J., Schlager, H., Schultz, M., Siegmund, P., Steil, B., Stephanou, E., Stier, P., Traub, M.,
25 Warneke, C., Williams, J., and Ziereis, H.: Global air pollution crossroads over the
26 Mediterranean, *Science*, 298, 794–799, doi: 10.1126/science.1075457, 2002.

27 Lopatin, A., Dubovik, O., Chaikovsky, A., Goloub, P., Lapyonok, T., Tanré, D., and Litvinov,
28 P.: Enhancement of aerosol characterization using synergy of lidar and sun-photometer
29 coincident observations: the GARRLiC algorithm, *Atmos. Meas. Tech.*, 6, 2065–2088,
30 doi:10.5194/amt-6-2065-2013, 2013.

- 1 Ming, Y., and L. M. Russell: Predicted hygroscopic growth of sea salt aerosol, *J. Geophys.*
2 *Res.*, 106(D22), 28259–28274, doi:10.1029/2001JD000454, 2001.
- 3 Mona, L., Amodeo, A., D’Amico, G., Giunta, A., Madonna, F., and Pappalardo, G.: Multi-
4 wavelength Raman lidar observations of the Eyjafjallajökull volcanic cloud over Potenza,
5 southern Italy, *Atmos. Chem. Phys.*, 12, 2229–2244, doi:10.5194/acp-12-2229-2012, 2012.
- 6 Mona, L., Papagiannopoulos, N., Basart Alpuente, S., Baldasano Recio, J. M., Biniotoglou, I.,
7 Cornacchia, C., & Pappalardo, G.: EARLINET dust observations vs. BSC-DREAM8b modeled
8 profiles: 12-year-long systematic comparison at Potenza, Italy. *Atmospheric chemistry and*
9 *physics*, 14(16), 8781-8793, 2014.
- 10 Monahan, E. C., Spiel, D. E., and Davidson, K. L.: A model of marine aerosol generation via
11 whitecaps and wave disruption, in: *Oceanic Whitecaps*, edited by: Monahan, E. C. and Mac
12 Niocaill, G., Reidel, D., 167–174, 1986.
- 13 Mishra, A. K., Klingmueller, K., Fredj, E., Lelieveld, J., Rudich, Y., and Koren, I.: Radiative
14 signature of absorbing aerosol over the eastern Mediterranean basin, *Atmos. Chem. Phys.*, 14,
15 7213-7231, doi:10.5194/acp-14-7213-2014, 2014.
- 16 Müller, D., Böckmann, C., Kolgotin, A., Schneidenbach, L., Chemyakin, E., Rosemann, J.,
17 Znak, P., and Romanov, A.: Microphysical particle properties derived from inversion
18 algorithms developed in the framework of EARLINET, *Atmos. Meas. Tech.*, 9, 5007-5035,
19 <https://doi.org/10.5194/amt-9-5007-2016>, 2016.
- 20 Nickovic, S., Kallos, G., Papadopoulos, A., and Kakaliagou, O.: A model for prediction of
21 desert dust cycle in the atmosphere, *J. Geophys. Res.*, 106, 18113–18130,
22 doi:10.1029/2000JD900794, 2001.
- 23 Otto, S., de Reus, M., Trautmann, T., Thomas, A., Wendisch, M., and Borrmann, S.:
24 Atmospheric radiative effects of an in situ measured Saharan dust plume and the role of large
25 particles, *Atmos. Chem. Phys.*, 7, 4887-4903, doi:10.5194/acp-7-4887-2007, 2007.
- 26 Papayannis, A., Balis, D., Amiridis, V., Chourdakis, G., Tsaknakis, G., Zerefos, C., Castanho,
27 A. D. A., Nickovic, S., Kazadzis, S., and Grabowski, J.: Measurements of Saharan dust aerosols
28 over the Eastern Mediterranean using elastic backscatter-Raman lidar, spectrophotometric and
29 satellite observations in the frame of the EARLINET project, *Atmos. Chem. Phys.*, 5, 2065-
30 2079, doi:10.5194/acp-5-2065-2005, 2005.

1 Papayannis, A., Nicolae, D., Kokkalis, P., Binetoglou, I., Talianu, C., Belegante, L., Tsaknakis.,
2 G., Cazacu, M. M., Vetres, I., and Ilic, I.: Optical, size and mass properties of mixed type
3 aerosols in Greece and Romania as observed by synergy of lidar and sunphotometers in
4 combination with model simulations: A case study, *Sci. Tot. Environ.*, 500–501, 277–294,
5 2014.

6 Pappalardo, G., Amodeo, A., Apituley, A., Comeron, A., Freudenthaler, V., Linné, H.,
7 Ansmann, A., Bösenberg, J., D’Amico, G., Mattis, I., Mona, L., Wandinger, U., Amiridis, V.,
8 Alados Arboledas, L., Nicolae, D., and Wiegner, M.: EARLINET: towards an advanced
9 sustainable European aerosol lidar network, *Atmos. Meas. Tech.*, 7, 2389–2409,
10 doi:10.5194/amt-7-2389-2014, 2014.

11 Pay, M. T., Piot, M., Jorba, O., Gassó, S., Gonçalves, M., Basart, S., Dabdub, D., Jiménez-
12 Guerrero, P., and Baldasano, J. M.: A full year evaluation of the CALIOPE-EU air quality
13 modeling system over Europe for 2004, *Atmos. Environ.*, 44, 3322–3342,
14 doi:10.1016/j.atmosenv.2010.05.040, 2010.

15 Pay, M. T., Jiménez-Guerrero, P., Jorba, O., Basart, S., Querol, X., Pandolfi, M., and Baldasano,
16 J. M.: Spatio-temporal variability of concentrations and speciation of particulate matter across
17 Spain in the CALIOPE modeling system, *Atmos. Environ.*, 46, 376–396, 2012.

18 Pérez, C., Nickovic, S., Pejanovic, G., Baldasano, J. M., and Ozsoy, E.: Interactive dust-
19 radiation modeling: a step to improve weather forecasts, *J. Geophys. Res.*, 11, D16206,
20 doi:10.1029/2005JD006717, 2006a.

21 Pérez, C., Nickovic, S., Baldasano, J. M., Sicard, M., Rocadenbosch, F., and Cachorro, V. E.:
22 A long Saharan dust event over the western Mediterranean: lidar, sun photometer observations,
23 and regional dust modeling, *J. Geophys. Res.*, 111, D15214, doi:10.1029/2005JD006579,
24 2006b.

25 Petters, M. D. and Kreidenweis, S. M.: A single parameter representation of hygroscopic
26 growth and cloud condensation nucleus activity, *Atmos. Chem. Phys.*, 7, 1961–1971,
27 doi:10.5194/acp-7-1961-2007, 2007.

28 Pielke, R. A., Cotton, W. R., Walko, R. L., Tremback, C. J., Lyons, W. A., Grasso, L. D.,
29 Nicholls, M. E., Moran, M. D., Wesley, D. A., Lee, T. J., and Copeland, J. H.: A comprehensive
30 meteorological modeling system—RAMS, *Meteor. Atmos. Phys.*, 49, 69–91, 1992.

1 Prospero, J. M.: Saharan dust transport over the North Atlantic Ocean and Mediterranean: an
2 overview, in: *The Impact of Desert Dust Across the Mediterranean* (eds. S. Guerzoni and R.
3 Chester), Kluwer Academic, Dordrecht, pp. 133–151, 1996.

4 Raptis, P. I., Kokkalis, P., Amiridis, V., Taylor, M. and Kazadzis, S.: A case study of columnar
5 marine and dust particle ratios calculated with photometric and lidar measurements during the
6 CHARADMEXP campaign, *EGU General Assembly Conference Abstracts*, 17, p. 8942, 2015.

7 Reid, J. S., Jonsson, H. H., Maring, H. B., Smirnov, A., Savoie, D. L., Cliff, S. S., Reid, E. A.,
8 Livingston, J. M., Meier, M. M., Dubovik, O., et al: Comparison of size and morphological
9 measurements of coarse mode dust particles from Africa. *J. Geophys. Res. Atmos.* 2003, 108,
10 doi:10.1029/2002JD002485, 2003.

11 Sciare J., Oikonomou, K., Favez, O., Markaki, Z., Liakakou, E., Cachier, H., and Mihalopoulos,
12 N.: Long-term measurements of carbonaceous aerosols in the Eastern Mediterranean: Evidence
13 of long-range transport of biomass burning, *Atmos. Chem. Phys.*, 8, 5551-5563, 2008.

14 Seinfeld, J. H. and Pandis, S. N.: *Atmospheric Chemistry and Physics: From Air Pollution to*
15 *Climate Change*, J. Wiley, Sons, Inc., New York, 1998.

16 Siomos, N., Balis, D. S., Poupkou, A., Liora, N., Dimopoulos, S., Melas, D., Giannakaki, E.,
17 Filioglou, M., Basart, S., and Chaikovsky, A.: Investigating the quality of modeled aerosol
18 profiles based on combined lidar and sunphotometer data, *Atmos. Chem. Phys.*, 17, 7003-7023,
19 <https://doi.org/10.5194/acp-17-7003-2017>, 2017.

20 Skamarock, W., Klemp, J. B., Dudhia, J., Gill, D. O., Barker, D., Duda, M. G., Huang, X. -Y.,
21 and Wang., W.: A description of the Advanced Research WRF version 3, NCAR Technical
22 Note NCAR/TN-475+STR, DOI: 10.5065/D68S4MVH, 2008.

23 Snider, J. R. and Petters, M. D.: Optical particle counter measurement of marine aerosol
24 hygroscopic growth, *Atmos. Chem. Phys.*, 8, 1949–1962, doi:10.5194/acp-8-1949-2008, 2008.

25 Solomos, S., Kallos, G., Kushta, J., Astitha, M., Tremback, C., Nenes, A., and Levin, Z.: An
26 integrated modeling study on the effects of mineral dust and sea salt particles on clouds and
27 precipitation, *Atmos. Chem. Phys.*, 11, 873-892, doi:10.5194/acp-11-873-2011, 2011.

28 Solomon, S., et al.: Intergovernmental Panel on Climate Change, *Climate Change 2007: The*
29 *Physical Science Basis. Contribution of Working Group I to the Fourth Assessment Report of*

1 the Intergovernmental Panel on Climate Change, Cambridge Univ Press, Cambridge, UK,
2 2007.

3 Stock, M., Cheng, Y. F., Birmili, W., Massling, A., Wehner, B., Müller, T., Leinert, S.,
4 Kalivitis, N., Mihalopoulos, N., and Wiedensohler, A.: Hygroscopic properties of atmospheric
5 aerosol particles over the Eastern Mediterranean: implications for regional direct radiative
6 forcing under clean and polluted conditions, *Atmos. Chem. Phys.*, 11, 4251-4271,
7 doi:10.5194/acp-11-4251-2011, 2011.

8 Tang, I.N., Tridico, A.C., and Fung, K. H.: Thermodynamic and optical properties of sea salt
9 aerosols, *J. Geophys. Res.*, 102(D19), 23269–23275, doi:10.1029/97JD01806, 1997.

10 Todd, M. C., Bou Karam, D., Cavazos, C., Bouet, C., Heinold, B., Baldasano, J. M., Cautenet,
11 G., Koren, I., Perez, C., Solmon, F., Tegen, I., Tulet, P., Washington, R., and Zakey, A.:
12 Quantifying uncertainty in estimates of mineral dust flux: an intercomparison of model
13 performance over the Bodélé Depression, northern Chad, *J. Geophys. Res.*, 113, D24107,
14 doi:10.1029/2008JD010476, 2008.

15 Tsekeri, A., Amiridis, V., Kokkalis, P., Basart, S., Chaikovsky, A., Dubovik, O., Mamouri, R.
16 E., Papayannis, A., and Baldasano, J. M.: Application of a Synergetic Lidar and Sunphotometer
17 Algorithm for the Characterization of a Dust Event Over Athens, Greece, *British J. of*
18 *Environment and Climate Change*, 3, 531–546, doi:10.9734/BJECC/2013/2615, 2013.

19 Tsekeri, A., Amiridis, V., Marengo, F., Nenes, A., Marinou, E., Solomos, S., Rosenberg, P.,
20 Trembath, J., Nott, G. J., Allan, J., Le Breton, M., Bacak, A., Coe, H., Percival, C., and
21 Mihalopoulos, N.: Profiling aerosol optical, microphysical and hygroscopic properties in
22 ambient conditions by combining in situ and remote sensing, *Atmos. Meas. Tech.*, 10, 83-107,
23 doi:10.5194/amt-10-83-2017, 2017.

24 Veselovskii, I., Goloub, P., Podvin, T., Bovchaliuk, V., Derimian, Y., Augustin, P., Fourmentin,
25 M., Tanre, D., Korenskiy, M., Whiteman, D. N., Diallo, A., Ndiaye, T., Kolgotin, A., and
26 Dubovik, O.: Retrieval of optical and physical properties of African dust from multiwavelength
27 Raman lidar measurements during the SHADOW campaign in Senegal, *Atmos. Chem. Phys.*,
28 16, 7013-7028, doi:10.5194/acp-16-7013-2016, 2016.

29 Vrekoussis M., Liakakou, E., Koçak, M., Kubilay, N., Oikonomou, K., Sciare J., and
30 Mihalopoulos, N.: Seasonal variability of optical properties of aerosols in the Eastern
31 Mediterranean, *Atmos. Environ.*, 39, 7083-7094, 2005.

1 Wagner, R., Ajtai, T., Kandler, K., Lieke, K., Linke, C., Müller, T., Schnaiter, M., and Vragel,
2 M.: Complex refractive indices of Saharan dust samples at visible and near UV wavelengths: a
3 laboratory study, *Atmos. Chem. Phys.*, 12, 2491-2512, [https://doi.org/10.5194/acp-12-2491-](https://doi.org/10.5194/acp-12-2491-2012)
4 2012, 2012.

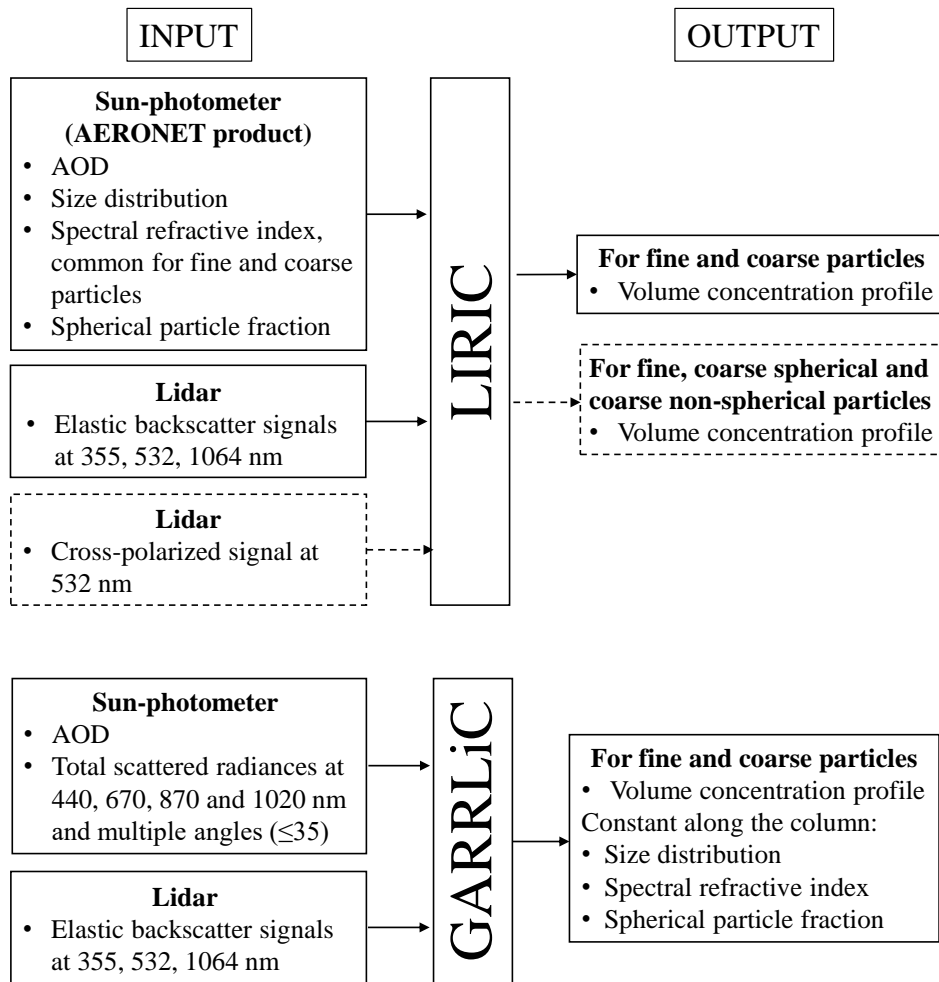
5 Wagner, J., Ansmann, A., Wandinger, U., Seifert, P., Schwarz, A., Tesche, M., Chaikovsky,
6 A., and Dubovik, O.: Evaluation of the Lidar/Radiometer Inversion Code (LIRIC) to determine
7 microphysical properties of volcanic and desert dust, *Atmos. Meas. Tech.*, 6, 1707–1724,
8 doi:10.5194/amt-6-1707-2013, 2013.

9 Wandinger U. and Ansmann A.: Experimental determination of the lidar overlap profile with
10 Raman lidar, *Appl. Opt.* 41, 511-514, 2002.

11 Zhang, K. M., Knipping, E. M., Wexler, A. S., Bhave, P. V., and Tonnesen, G. S.: Size
12 distribution of sea-salt emissions as a function of relative humidity, *Atmos. Environ.*, 39, 3373-
13 3379, 2005.

14

15



1

2

3 Figure 1. GARRLiC and LIRIC algorithm input and output parameters. For LIRIC, the output

4 in case of using the cross-polarized signal at 532 nm is shown in the dashed box.



1

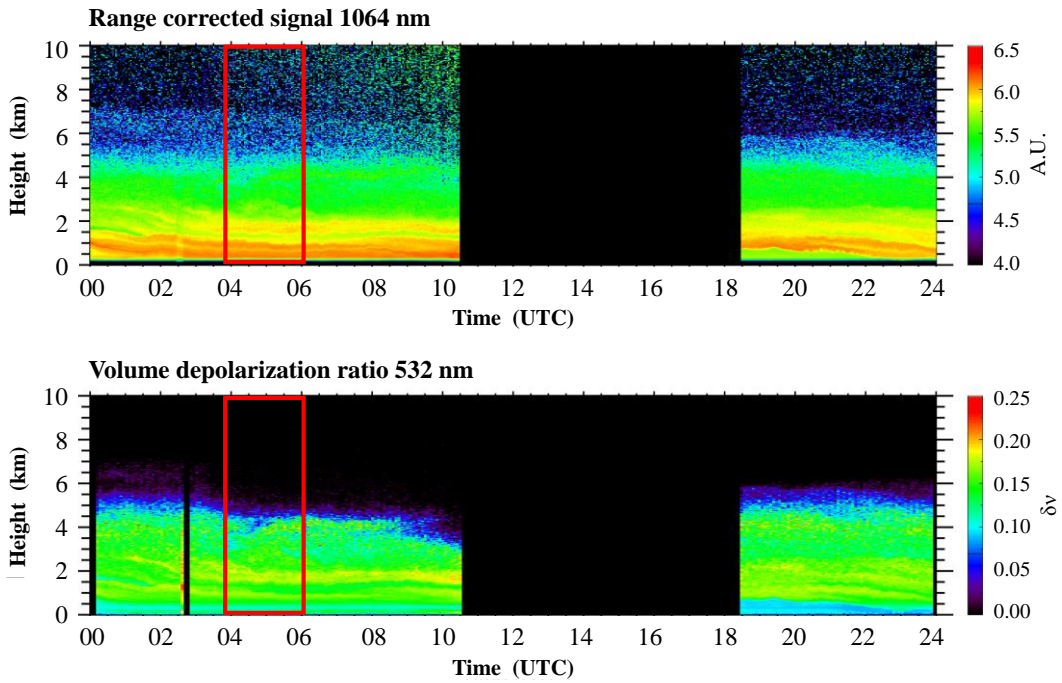
a)

b)

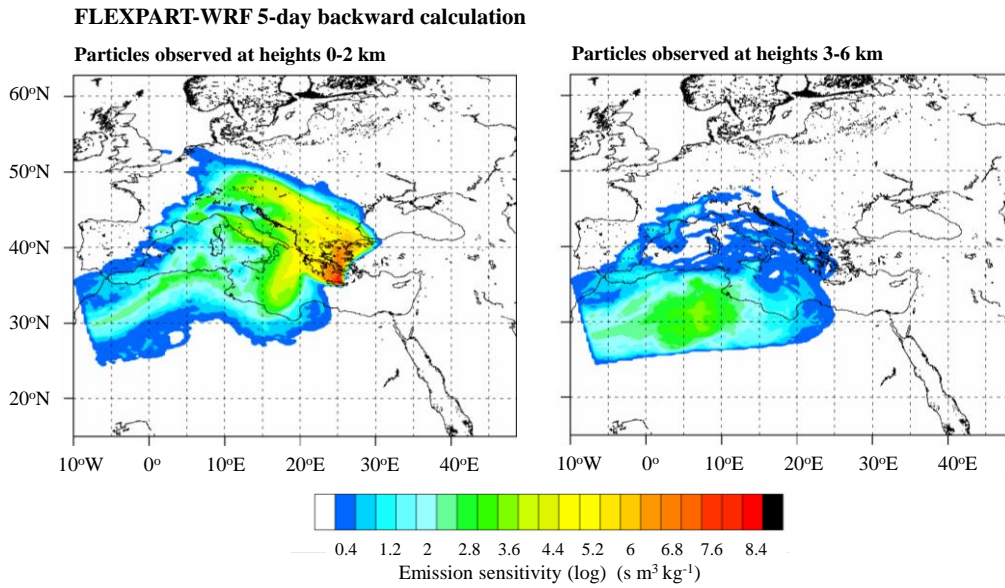
2

3 Figure 2. a) Location of Finokalia station (red dot) in Crete island, Greece. b) Sea view from
4 the station.

5



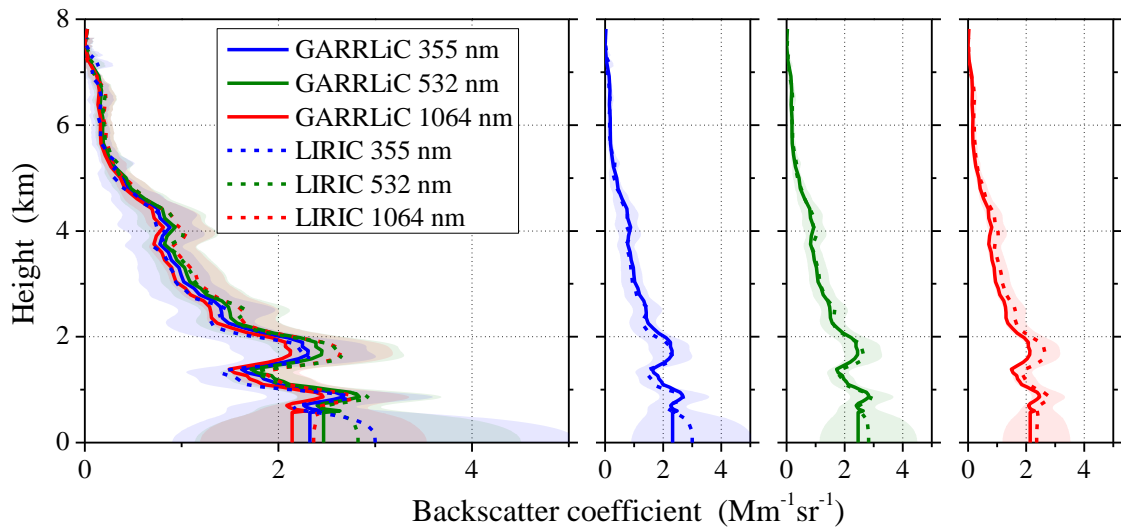
1 a)



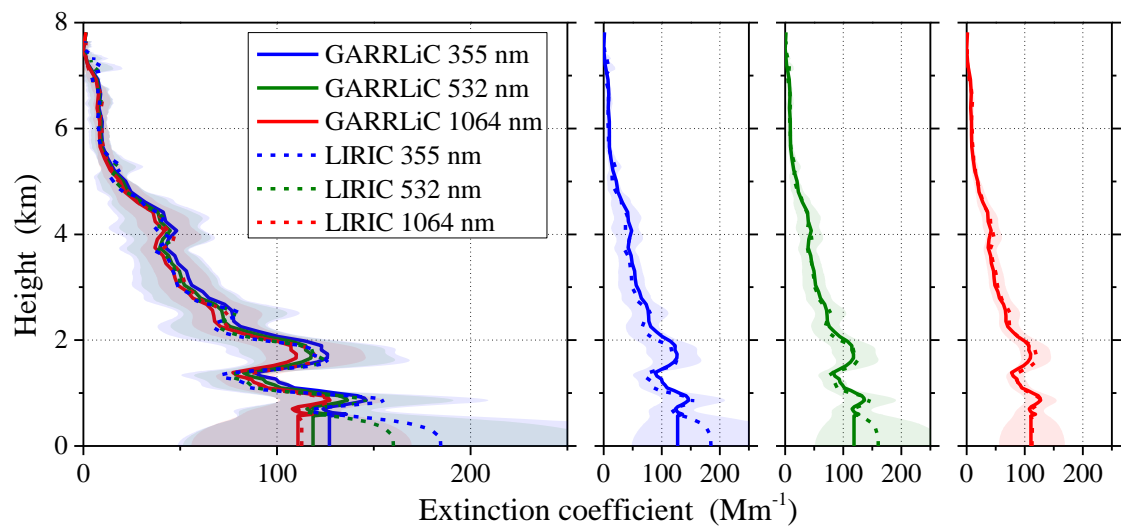
2 b)

3

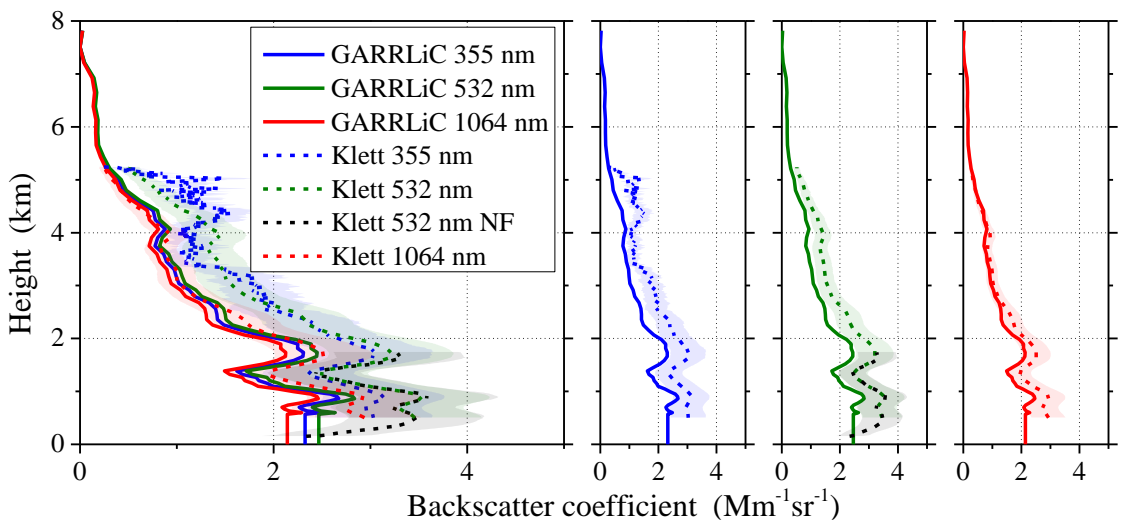
4 Figure 3. a) Range-corrected backscattered signal at 1064 nm in arbitrary units (top) and volume
 5 depolarization ratio at 532 nm (bottom) from Polly^{XT} OCEANET lidar, at Finokalia, Crete, on
 6 June 26, 2014. The red rectangle indicates the time range of the measurements used for
 7 GARRLiC and LIRIC retrievals (04:00-06:00 UTC). b) Five day backward FLEXPART-WRF
 8 calculation of emission sensitivity (i.e., residence time in the lowest 1 km in the atmosphere) in
 9 $\log(\text{s m}^3 \text{ kg}^{-1})$ for the particles arriving at 0-2 km (left) and 3-6 km (right) at 04:00 UTC.



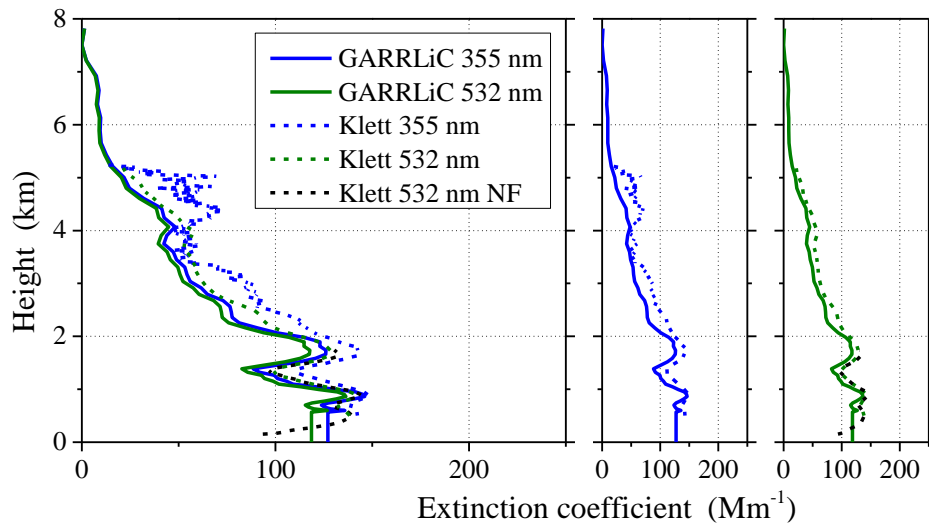
1 a)



2 b)



3 c)

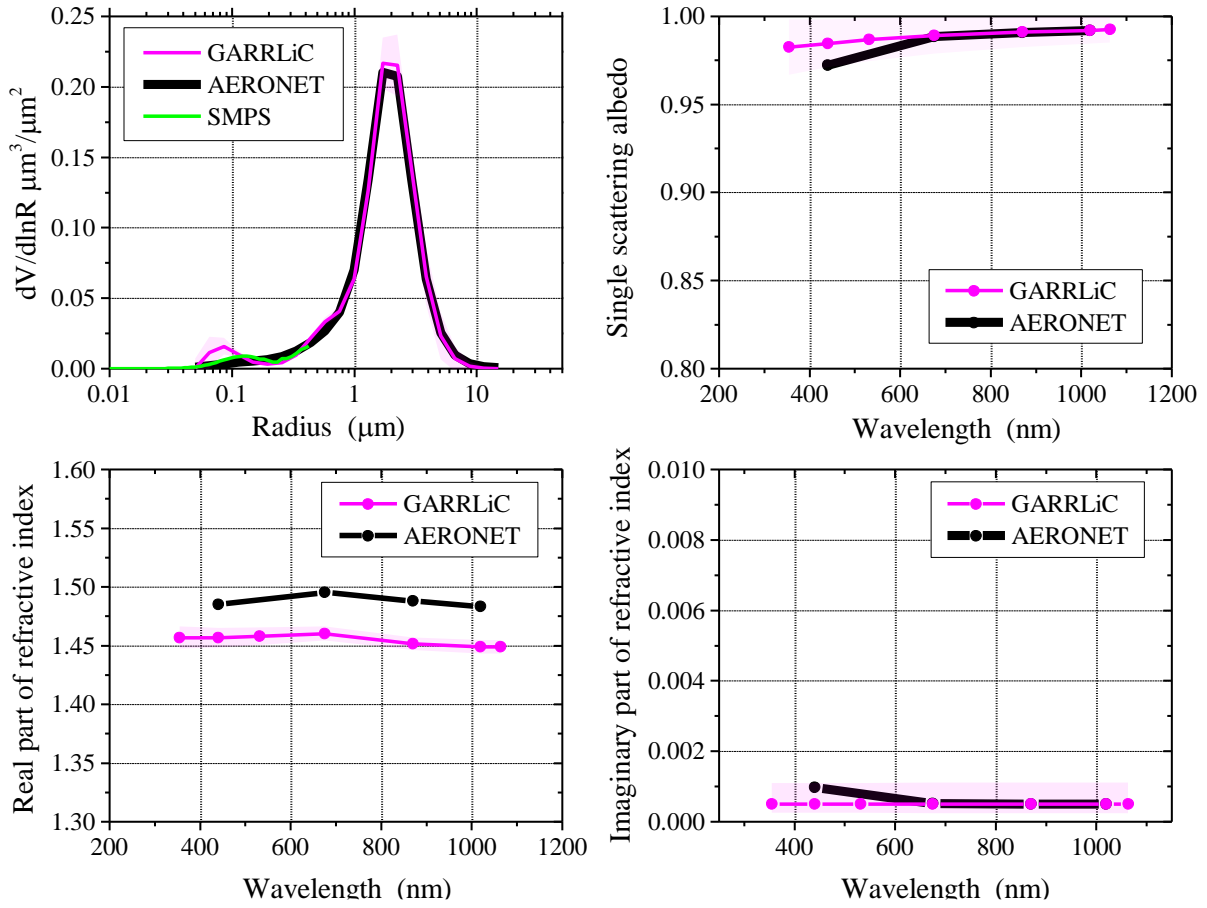


1 d)

2

3 Figure 4: Backscatter and extinction coefficient retrievals, at Finokalia, Crete, on June 26, 2014,
 4 at 04:00-06:00 UTC. a) and b): Backscatter and extinction coefficients from GARRLiC and
 5 LIRIC. c) and d): Backscatter and extinction coefficients from GARRLiC and Klett. In each
 6 row the first plot contains the results for all wavelengths (i.e., 355, 532 and 1064 nm) and the
 7 next three plots contain the results for each wavelength separately.

8

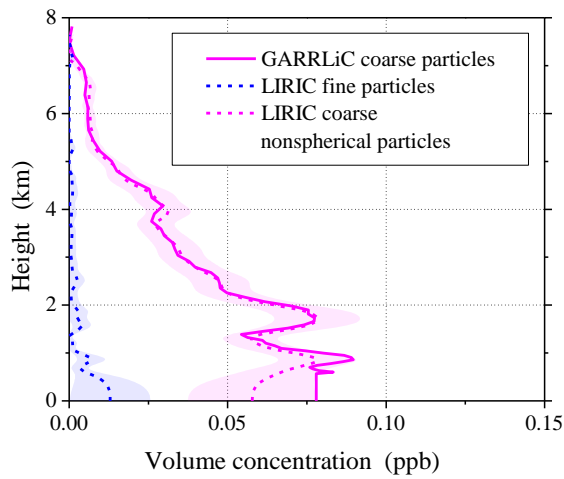


1

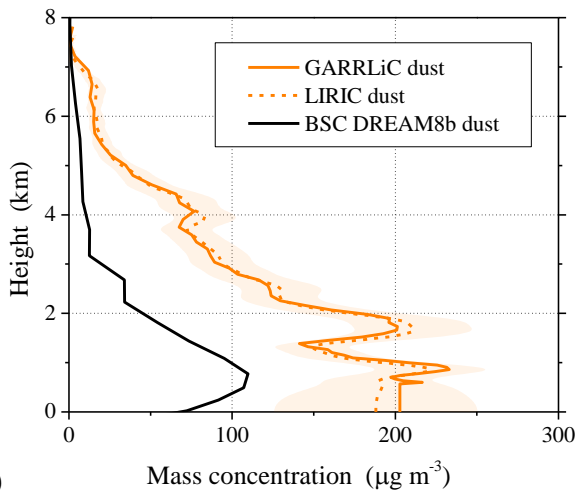
2

3 Figure 5: GARRLiC retrievals (pink) of size distribution (up-left), spectral SSA (up-right),
 4 spectral real and imaginary part of the refractive index (bottom –left and right), on June 26,
 5 2014, at 04:00-06:00 UTC, in Finokalia, Crete. The black line shows the AERONET retrieval
 6 at 04:54 UTC (used also in LIRIC). The green line in the size distribution plot (up-left) is the
 7 mean value of the surface in situ SMPS measurements at 04:00-06:00 UTC.

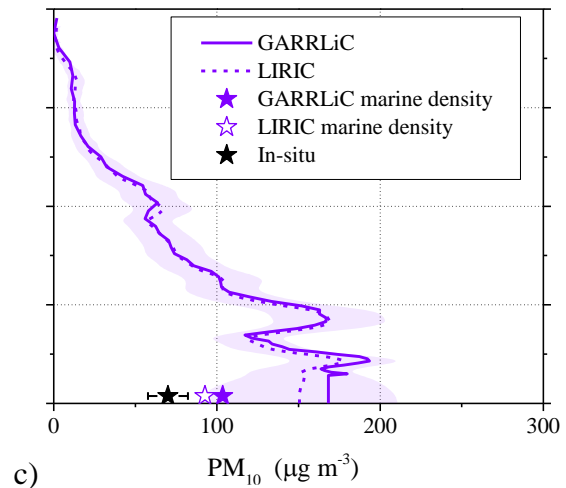
8



1 a)



2 b)

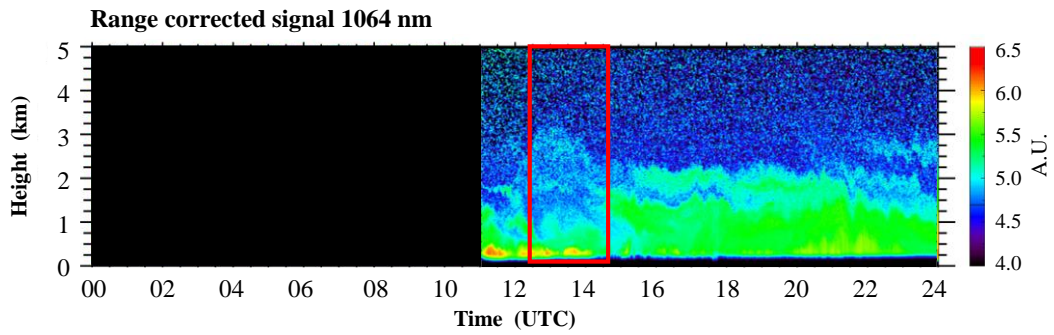


3 c)

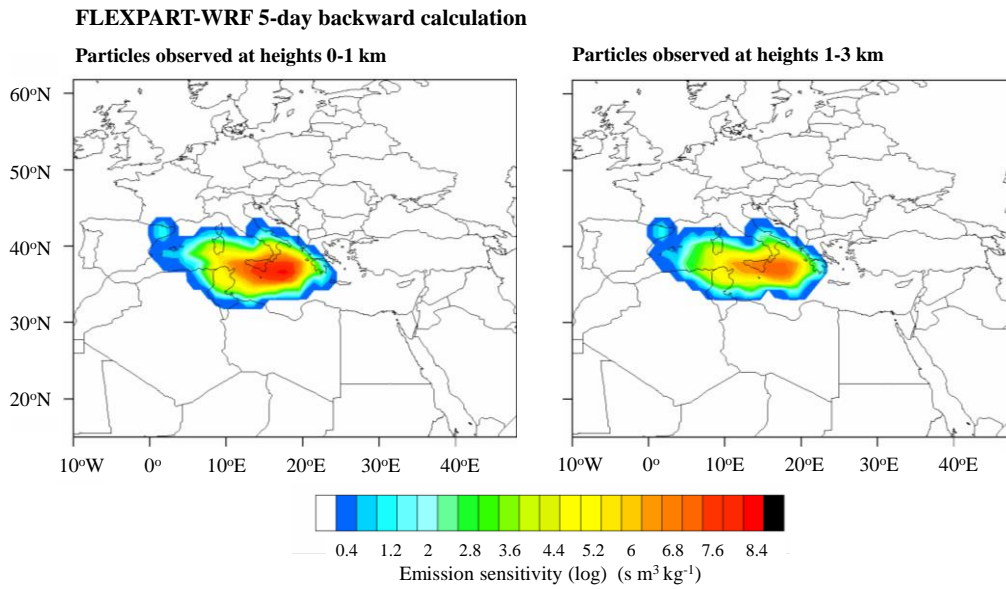
4

5 Figure 6: a) Volume concentration profiles for GARRLiC coarse particles (pink), and LIRIC
6 fine (dash blue) and coarse nonspherical particles (dash pink), on June 26, 2014, at 04:00-06:00
7 UTC, in Finokalia, Crete. b) Dust mass concentration profiles from GARRLiC (orange), LIRIC
8 (dash orange) and BSC DREAM8b model (black) (the latter at 05:00 UTC). c) PM₁₀ profiles
9 from GARRLiC (purple) and LIRIC (dash purple), along with their surface values, considering
10 only marine particles at the surface (“GARRLiC marine density” and “LIRIC marine density”
11 denoted by purple star and white star, respectively). The black star denotes the surface in situ
12 measurements at 05:00-06:00 UTC (mean and time variability).

12



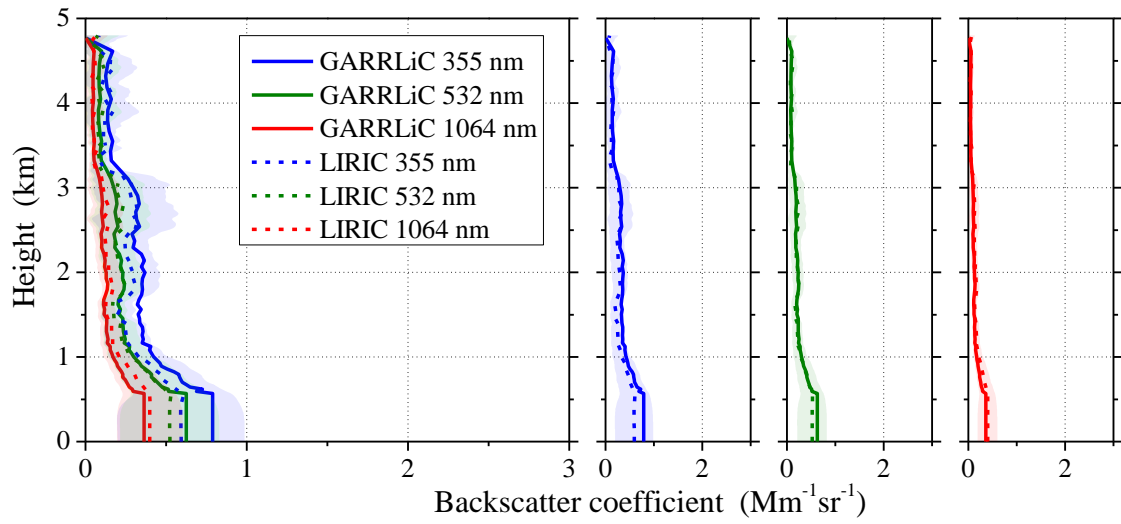
1 a)



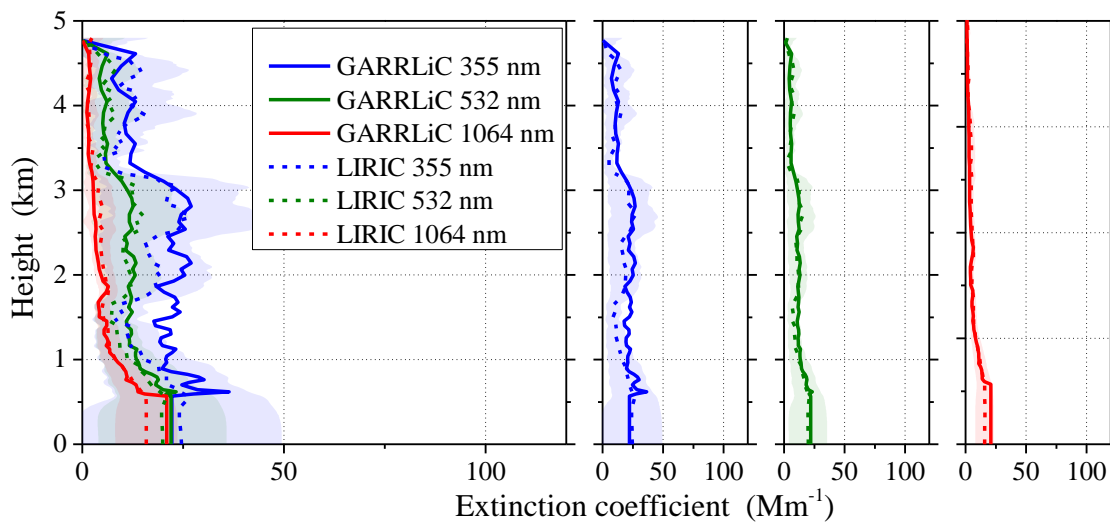
2 b)

3

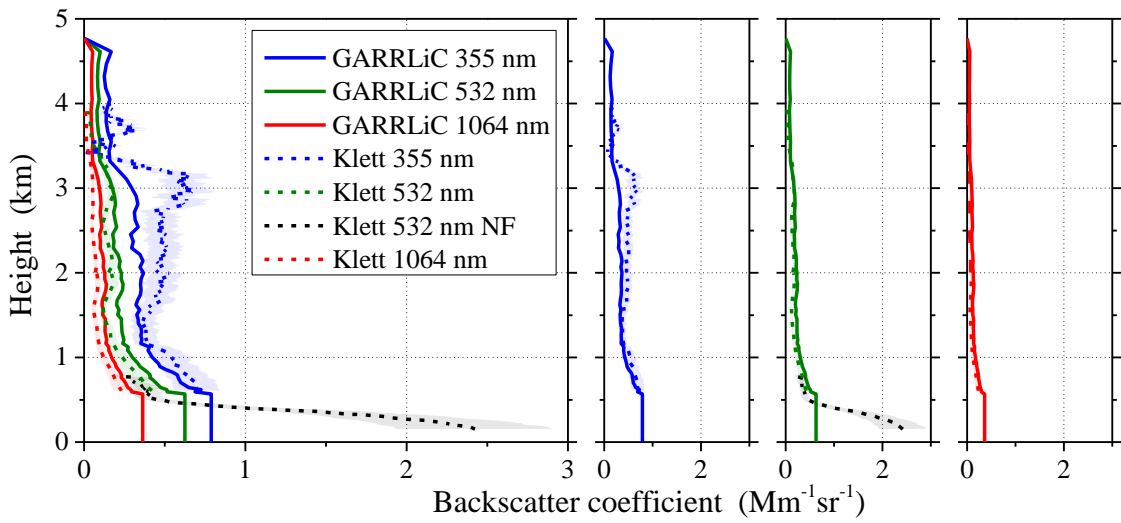
4 Figure 7. a) Range-corrected backscattered signal at 1064 nm in arbitrary units from Polly^{XT}
 5 OCEANET lidar, at Finokalia, Crete, on July 15, 2014. The red rectangle indicates the time
 6 range of the measurements used for the GARRLiC and LIRIC retrievals (12:30-14:30 UTC).
 7 b) Five day backward FLEXPART-WRF calculation of emission sensitivity (i.e., residence
 8 time in the lowest 1 km in the atmosphere) in $\log(\text{s m}^3 \text{kg}^{-1})$ for the particles arriving at the
 9 layers 0-1 km (left) and 1-3 km (right) at 14:00 UTC.



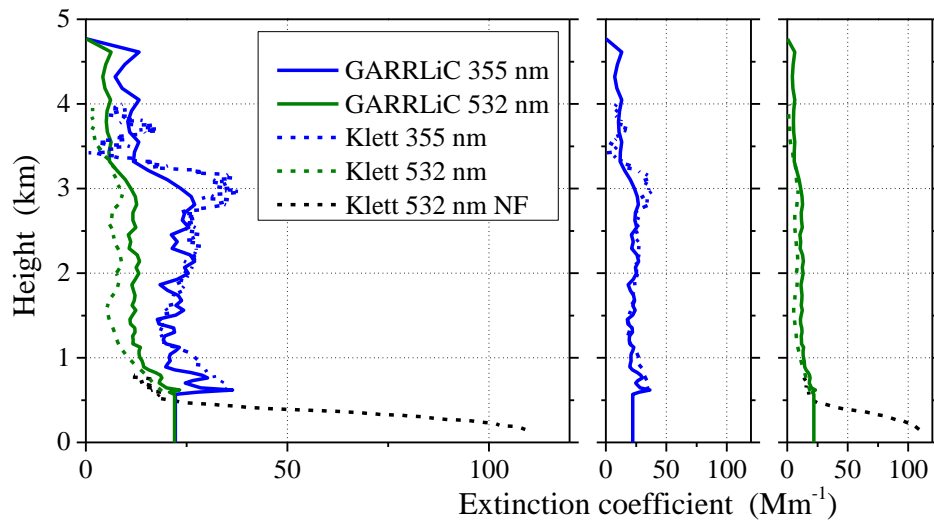
1 a)



2 b)



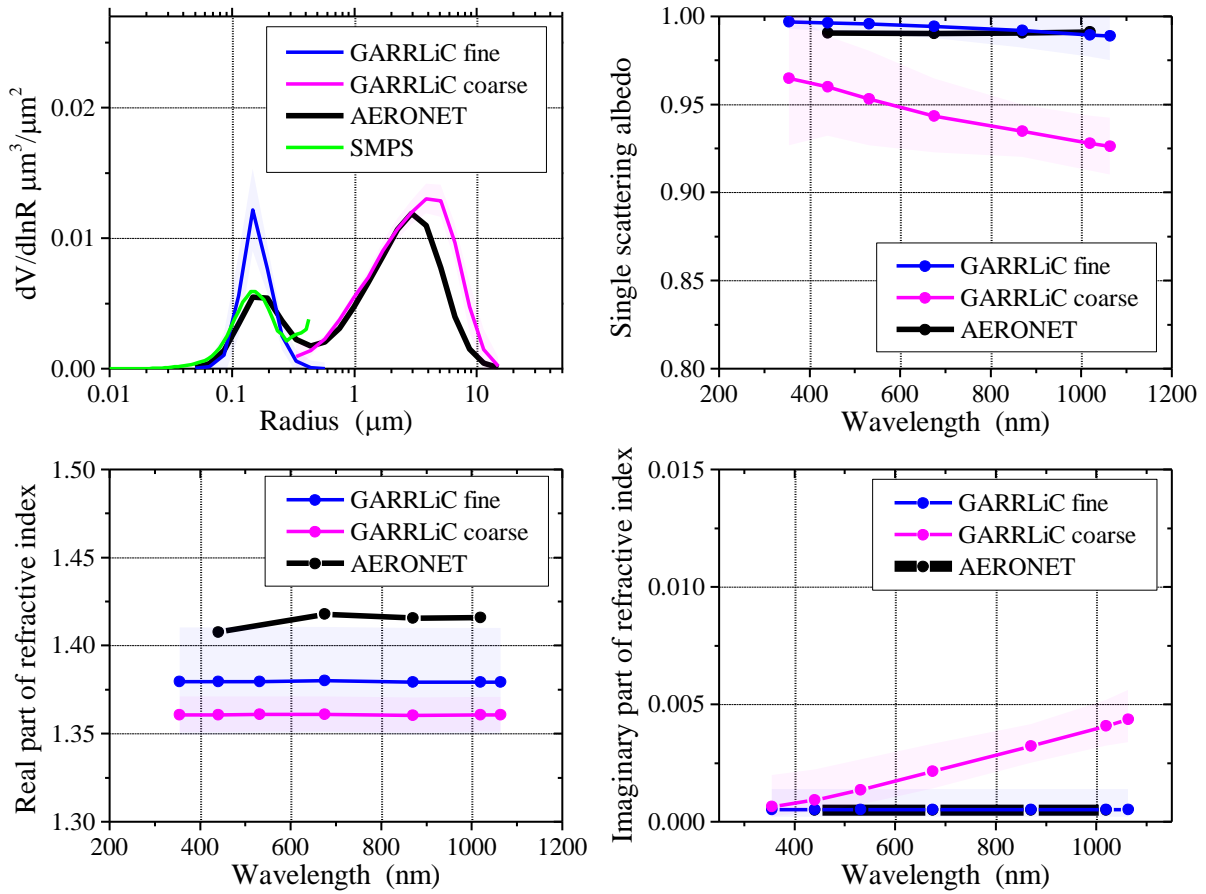
3 c)



1 d)

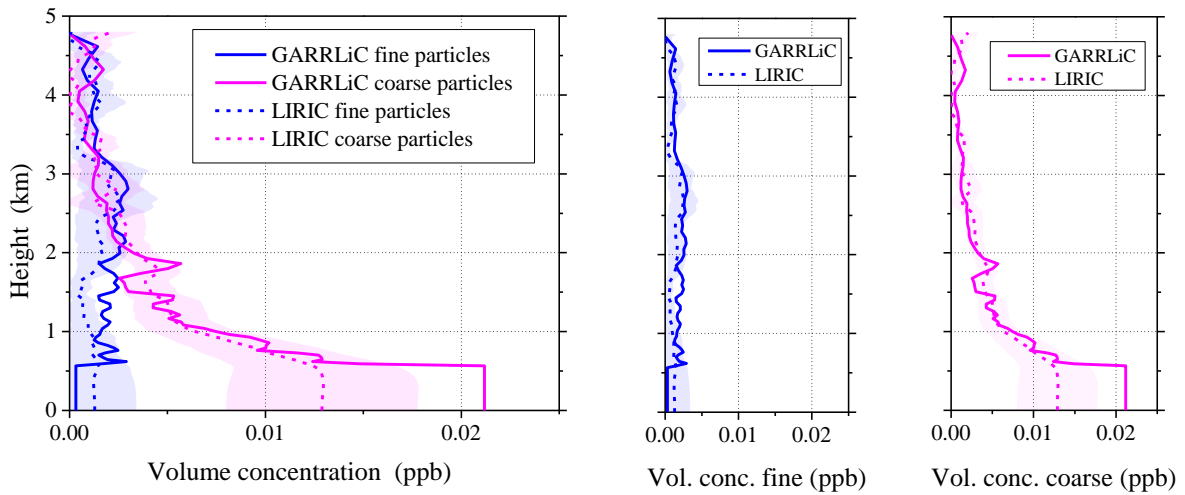
2

3 Figure 8: As in Fig. 4 for backscatter and extinction coefficient retrievals at Finokalia, Crete,
 4 on July 15, 2014, at 12:30-14:30 UTC.

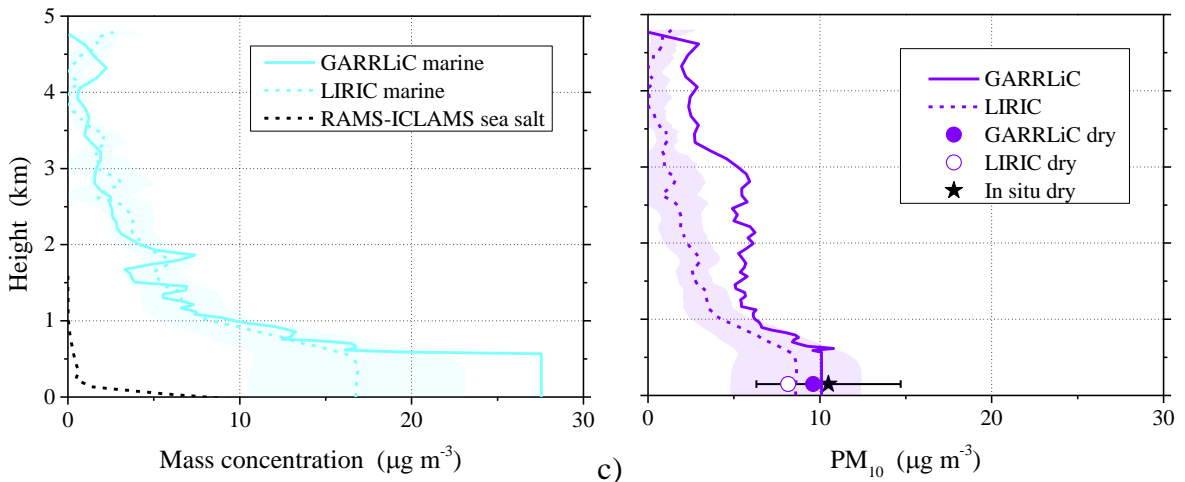


1
2
3
4
5
6
7
8

Figure 9: GARRLiC retrievals for fine (blue) and coarse particles (pink) of size distribution (up-left), spectral SSA (up-right), spectral real and imaginary part of the refractive index (bottom –left and right), at Finokalia, Crete, on July 15, 2014, at 12:30-14:30 UTC. The black line shows the AERONET retrieval at 13:24 UTC. The green line in the size distribution plot (up-left) is the mean value of the surface in situ SMPS measurements at 12:00-13:20 UTC.



1 a)



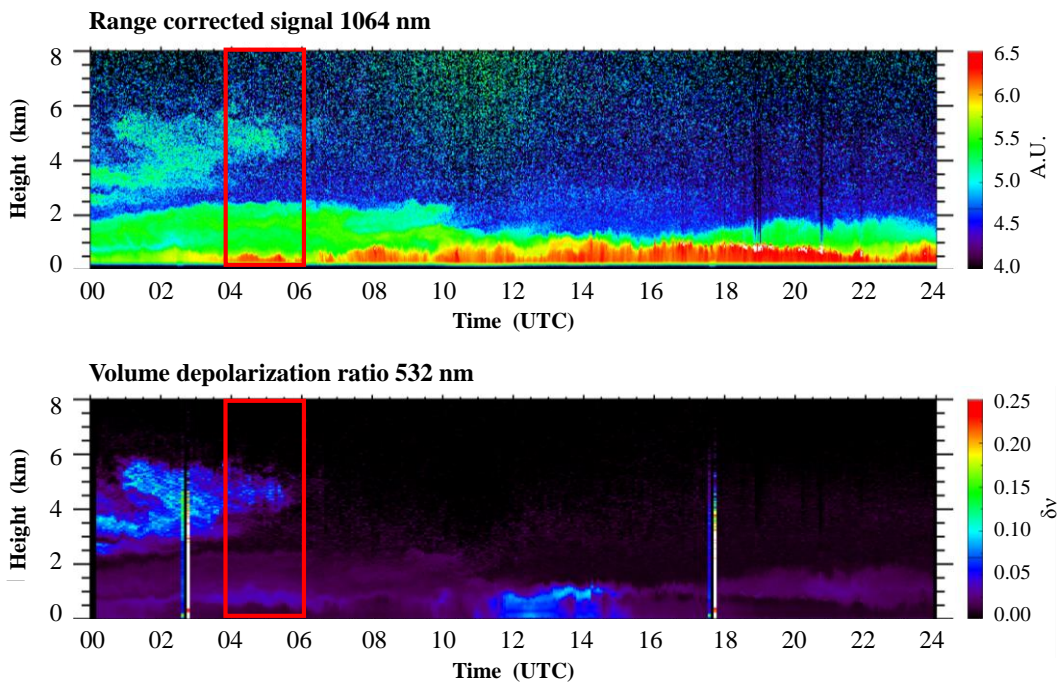
2 b)

c)

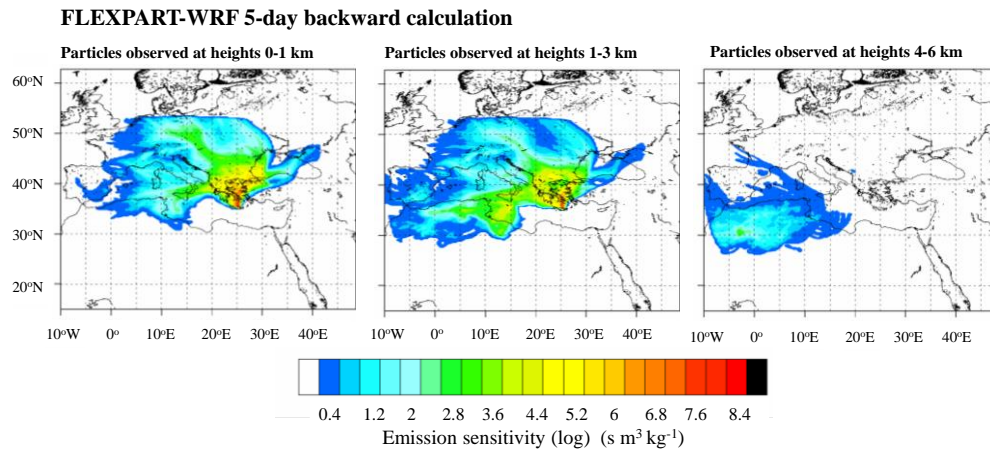
3

4 Figure 10: a) Volume concentration profiles for GARRLiC fine (blue) and coarse particles
 5 (pink) and LIRIC fine (dash blue) and coarse spherical particles (dash pink), at Finokalia, Crete,
 6 on July 15, 2014, at 12:30-14:30 UTC. b) GARRLiC (light blue) and LIRIC (dash light blue)
 7 marine particle mass concentration profiles, along with the RAMS-ICLAMS sea salt mass
 8 concentration profile (black) at 13:00 UTC. c) PM₁₀ profiles from GARRLiC (purple) and
 9 LIRIC (dash purple), along with the “dry” GARRLiC and LIRIC PM₁₀ at the surface (purple
 10 and white circles, respectively). The black star denotes the in situ PM₁₀ measurements at 4-5
 11 UTC (mean and time variability).

12



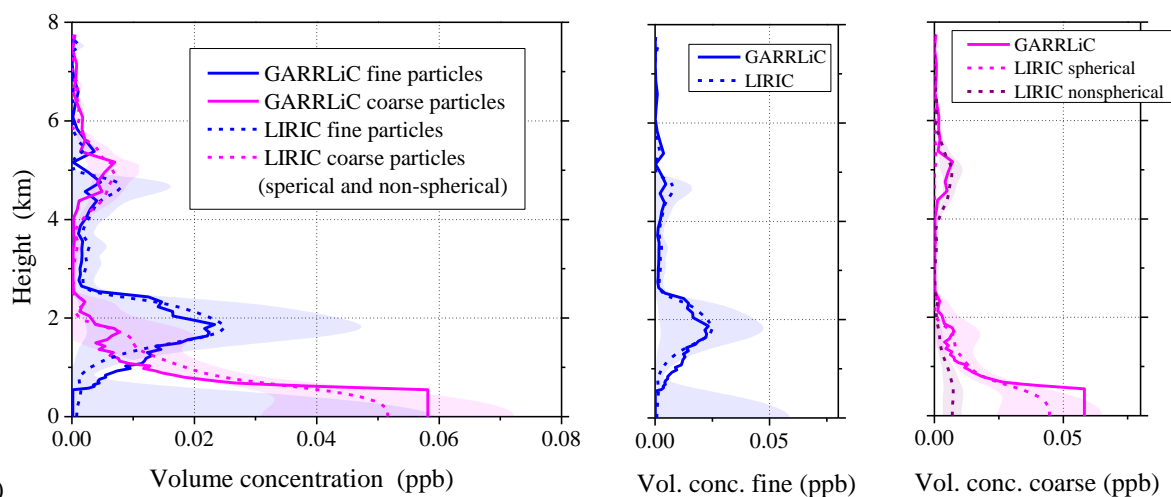
1 a)



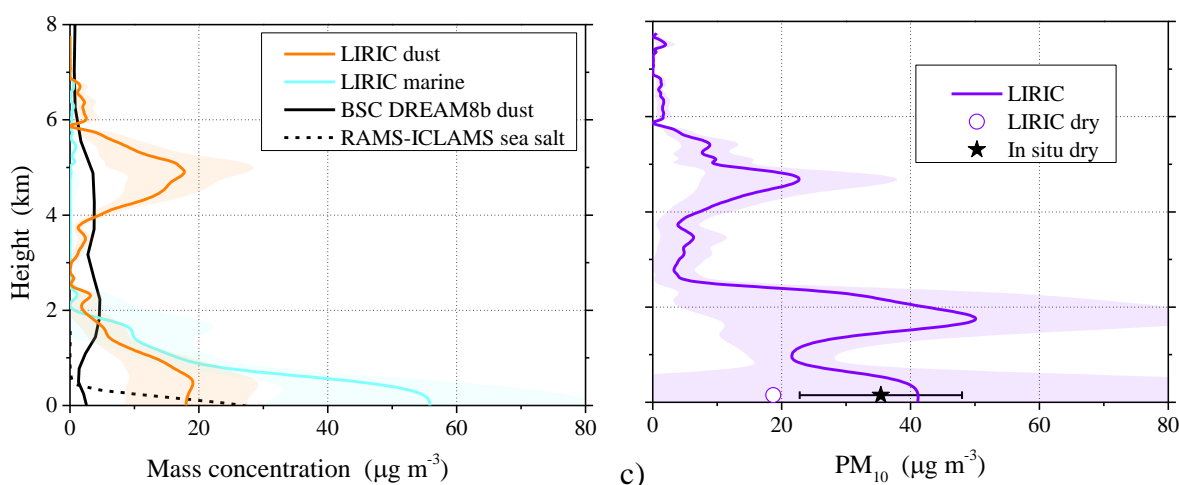
2 b)

3

4 Figure 11: a) Range-corrected backscattered signal at 1064 nm in arbitrary units (top) and
 5 volume depolarization ratio at 532 nm (bottom) from Polly^{XT} OCEANET lidar, at Finokalia,
 6 Crete, on July 4, 2014. The red rectangle indicates the GARRLiC and LIRIC retrievals (04:00-
 7 06:00 UTC). b) Five day backward FLEXPART-WRF calculation of emission sensitivity (i.e.,
 8 residence time in the lowest 1km in the atmosphere) in $\log(\text{s m}^3 \text{ kg}^{-1})$ for the particles arriving
 9 at heights 0-1 km (left), 1-3 km (middle) and 4-6 km (right), at 07:00 UTC.

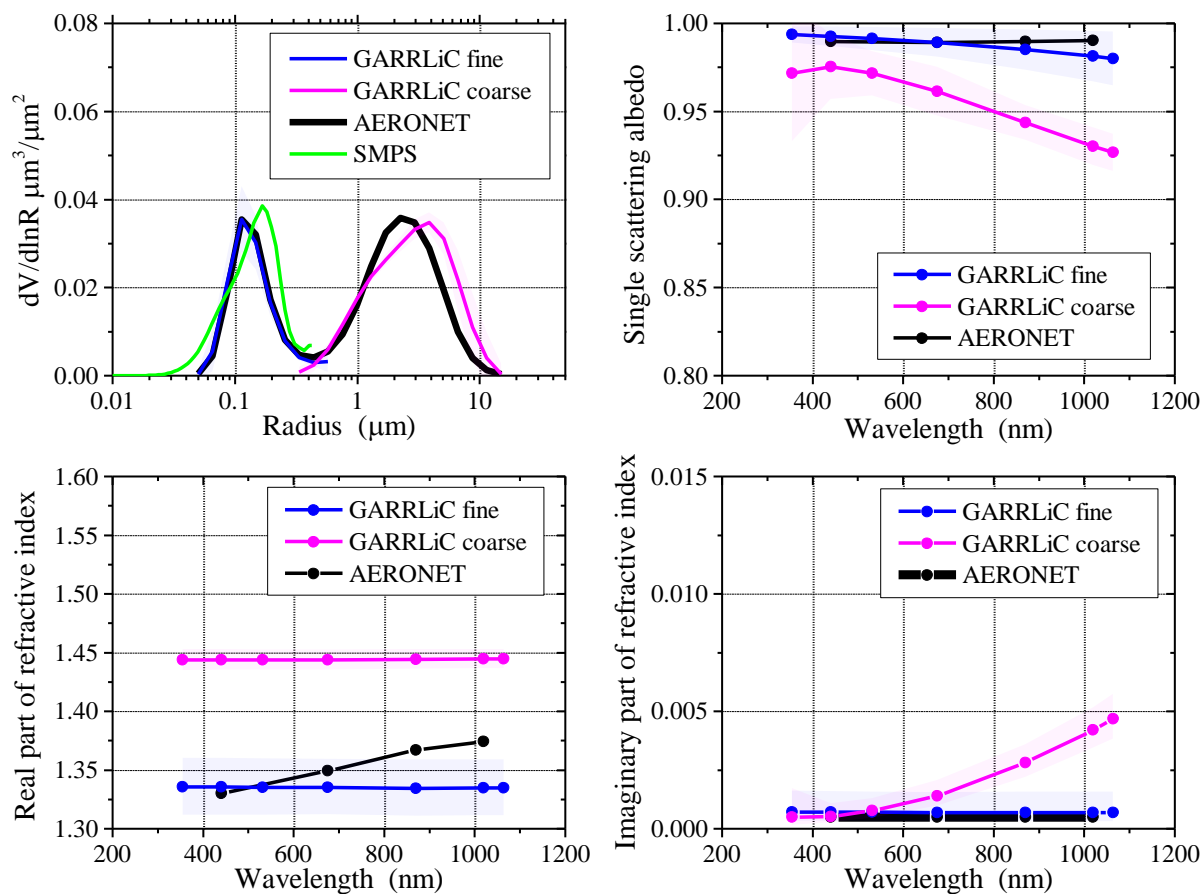


1 a)
2



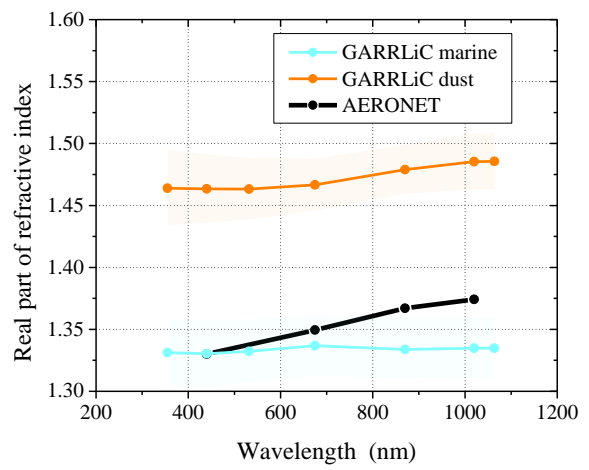
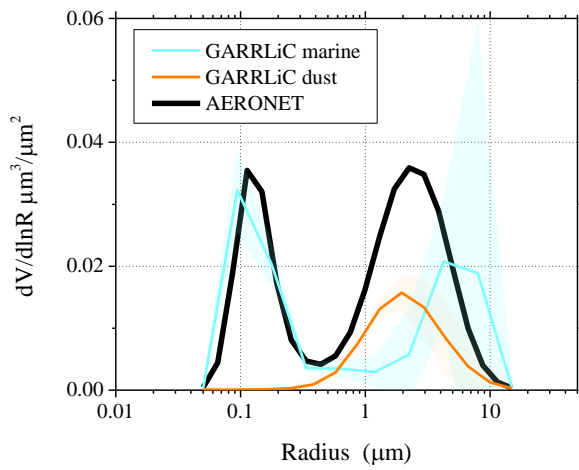
3 b)
4

5 Figure 12: a) Left: Volume concentration profiles for GARRLiC fine (blue) and coarse particles
6 (pink) and LIRIC fine (dash blue) and total coarse particles (dash pink), at Finokalia, Crete, on
7 July 4, 2014, at 04:00-06:00 UTC. Middle: Volume concentration of fine particles from
8 GARRLiC (blue) and LIRIC (dash blue). Right: Volume concentration of coarse particles from
9 GARRLiC (pink) and LIRIC, disentangled in the spherical (dash pink) and non-spherical (dash
10 purple) components. b) Mass concentration profiles for LIRIC dust (orange) and marine
11 particles (light blue), along with the modelled dust (black) and sea salt (dash black) particle
12 concentration profiles (both at 05:00 UTC). c) PM₁₀ profile from LIRIC (purple), along with
13 the “dry” LIRIC PM₁₀ at the surface (white circle). The black star denotes the surface in situ
14 PM₁₀ measurements at 4-5 UTC (mean and time variability).
15



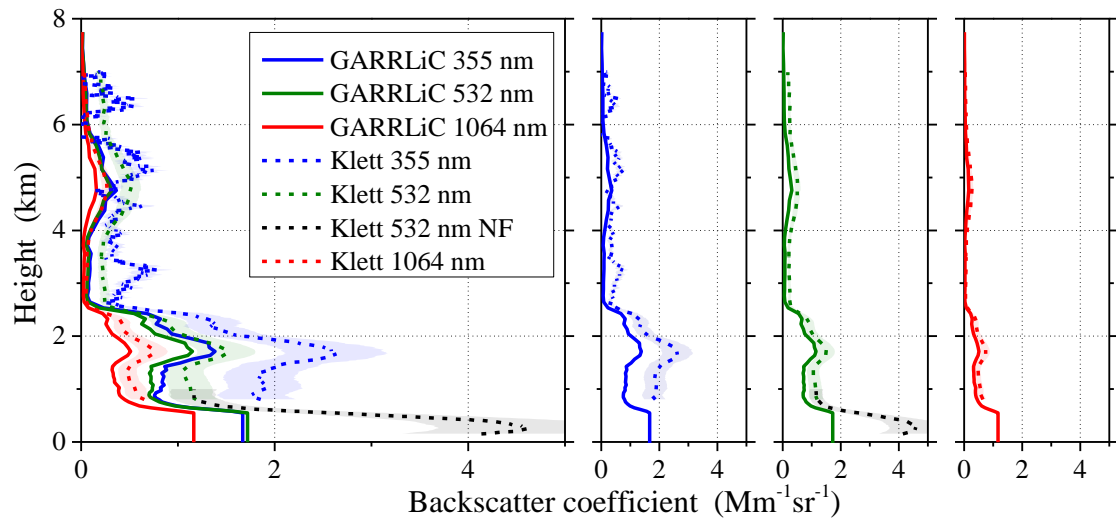
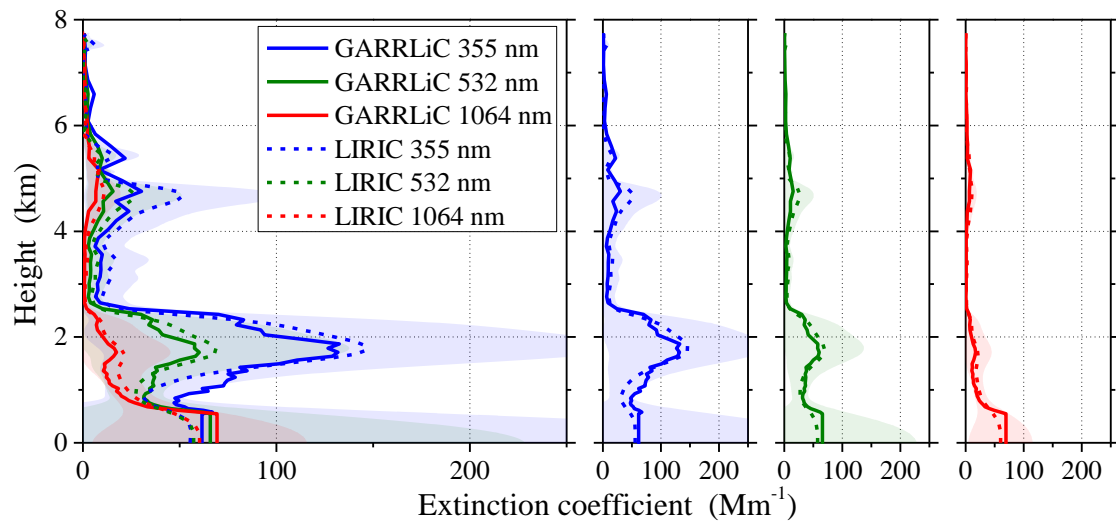
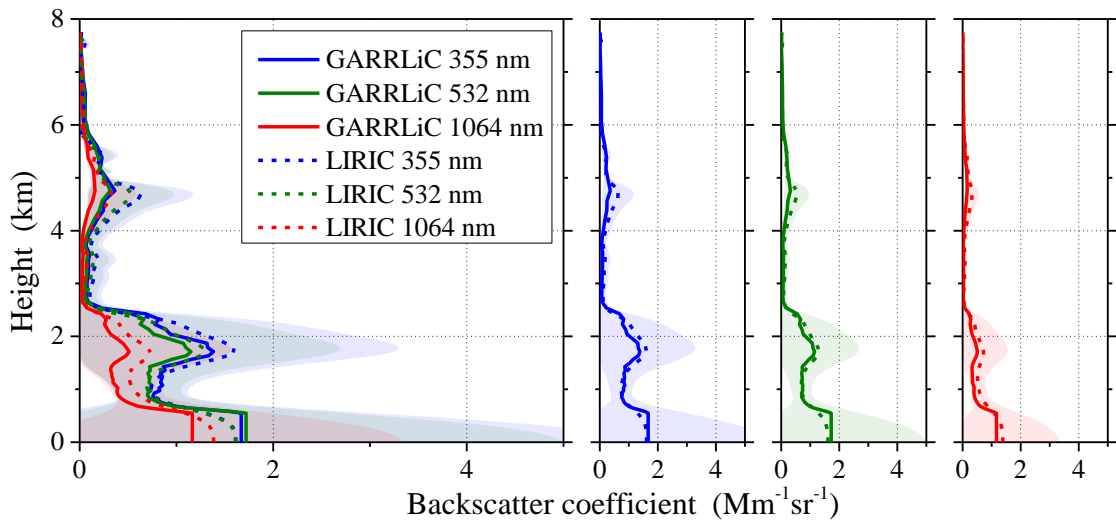
1
2
3
4
5
6
7
8
9

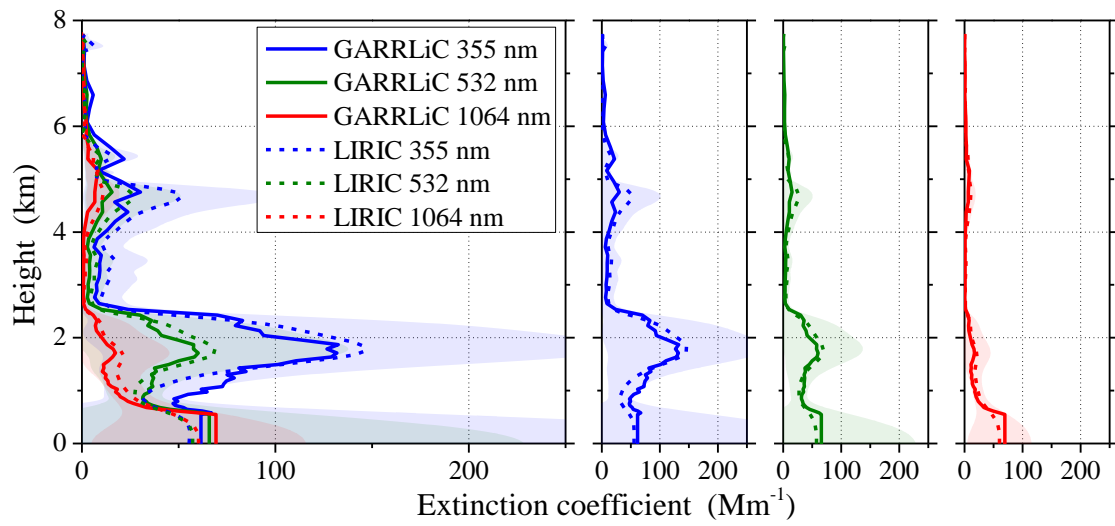
Figure 13: GARRLiC retrievals for fine (blue) and coarse particles (pink) of size distribution (up-left), spectral SSA (up-right), spectral real and imaginary part of the refractive index (bottom –left and right), at Finokalia, Crete, on July 4, 2014, at 04:00-06:00 UTC. The black line shows the AERONET retrieval at 05:49 UTC. The green line in the size distribution plot (up-left) is the mean value of the surface in situ SMPS measurements at 04:00-06:00 UTC.



1
2
3
4
5
6
7

Figure 14: Potential of GARRLiC to retrieve “marine” (light blue) and “dust” particle (orange) size distribution (left) and spectral real part of the refractive index (right). The retrieval refers to measurements at Finokalia, Crete, on July 4, 2014, at 04:00-06:00 UTC. The black line shows the AERONET retrieval at 05:49 UTC.





1 d)

2

3 Figure 15: As in Fig. 4 for backscatter and extinction coefficient retrievals at Finokalia, Crete,
 4 on July 4, 2014, at 04:00-06:00 UTC.